FACULDADE DE ENGENHARIA DA UNIVERSIDADE DO PORTO

Thermal optimization of deposition during robotic 3D printing of large parts

Diana Filipa Gonçalves Martins

Mestrado Integrado em Engenharia Mecânica

Supervisor: Prof. Fernando Gomes de Almeida

Co-Supervisor at INEGI: Dr. Luís Miguel da Quinta e Costa Neves de Oliveira

Co-Supervisor at INEGI: Eng. João Rui Barros Matos

June, 2023

Thermal optimization of deposition during robotic 3D printing of large parts

Diana Filipa Gonçalves Martins

Mestrado Integrado em Engenharia Mecânica

June, 2023

Abstract

Applications that take advantage of 3D printing have been increasing, but there is a size limit in conventional Fused Deposition Modeling (FDM) techniques. The robotic system on which this work was developed attempts to solve this problem by increasing the size and quantity of the deposited material. As the size and quantity of material increases and, because the thermal conductivity of thermoplastics is low, the printed object stays hot for a long time. This results in printing failure, since the previously deposited layers can't handle the weight of more material on top, causing them to collapse.

After some attempts to solve this issue at INEGI, the implementation of a thermal camera based solution was proposed. First, a support to attach the camera to the robot was designed. Afterwards, an application was developed in order to enable the computation of the data acquired by the camera. Alongside this step, the routine of the robot was modified so that after depositing a layer, the robot would position the camera in order to get the temperature of the deposited layer. When the layer reached an acceptable temperature, the printing could continue until the object was fully built.

The system modifications worked as intended. After running experiments with and without the temperature optimization it was possible to compare the resulting printed objects. The one printed without temperature control failed, resulting in the collapse of its walls during the printing process. The object printed with the temperature control was successfully built, suggesting that this solution can be used for large-scale 3D printing.

Keywords: large-scale 3D printing , thermal optimization, thermal camera process

Resumo

As aplicações que tiram partido da impressão 3D têm vindo a aumentar, mas existe um limite de tamanho nas técnicas convencionais de Fused Deposition Modeling (FDM). O sistema robótico em que este trabalho foi desenvolvido tenta resolver este problema aumentando o tamanho e a quantidade do material depositado. À medida que o tamanho e a quantidade de material aumentam, e porque a condutividade térmica dos termoplásticos é baixa, o objecto impresso permanece quente durante muito tempo. Isto resulta numa falha de impressão, uma vez que as camadas previamente depositadas não conseguem suportar o peso de mais material por cima, provocando o seu colapso.

Depois de algumas tentativas para resolver este problema no INEGI, a implementação de uma solução baseada numa câmara térmica foi proposta. Primeiro, foi concebido um suporte para fixar a câmara ao robot. Posteriormente, foi desenvolvida uma aplicação para permitir a computação dos dados adquiridos pela câmara. Paralelamente a este passo, a rotina do robot foi modificada de modo a que, após depositar uma camada, o robot posicionasse a câmara de modo a obter a temperatura da camada depositada. Quando a camada atingia uma temperatura aceitável, a impressão podia continuar até o objecto estar totalmente construído.

As modificações do sistema funcionaram como pretendido. Após a realização de experiências com e sem a optimização da temperatura, foi possível comparar os objectos impressos resultantes. O objecto impresso sem controlo de temperatura falhou, resultando no colapso das suas paredes durante o processo de impressão. Já o objecto impresso com controlo de temperatura foi construído com sucesso, sugerindo que esta solução poderá ser utilizada para impressão 3D em larga escala.

Keywords: impresão 3D grandes dimensões, otimização térmica, processo com camera térmica

Acknowledgements

I would like to express my appreciation to all the people who have played a vital role in the completion of this dissertation. My sincere thanks:

In first place, to my parents. For all the effort and motivation they offer to me at all times. Their love and guidance have been the driving force behind my growth as an individual.

To my Supervisor, Professor Fernando Gomes de Almeida, for the share of knowledge and involvement on this thesis. It was an honor working under his supervision.

To my Co-Supervisor Dr. Luís Miguel Oliveira, for giving me the opportunity to grow as a student. For always giving such great suggestions for this project and also, for keeping his attention on my work.

To my Co-Supervisor Eng. João Rui Matos for always tracking my progress and transmitting powerful knowledge. His commitment to this project is invaluable and I will always be thankful for his dedicated efforts.

To INEGI members, specially to Eng. Catarina Costa and Eng. Miguel Ferreira, for always being available to help me overcome my difficulties.

To Henrique, for all the time spent teaching me valuable programming skills. And also for all the encouragement and love.

To all my friends and my brother, Ricardo, for always supporting and believing in me.

Thank you so much!

Diana Martins
Junho 2023

"The journey of a thousand miles must begin
with a single step."

Lao Tzu

Contents

List of Figures

List of Tables

Abbreviations

ABS	Acrylonitrile Butadiene Styrene
AM	Additive Manufacturing
ADS	Automation Device Specification
CAD	Computer Aided-Design
EAP	EtherCAT Automation Protocol
FDM	Fused Deposition Modelling
FGB	Fibre Bragg Grating
FOV	Field of View
HMI	Human-Machine Interface
IR	Infrared
PHA	Polyhydroxyalkanoates
ROI	Region Of Interest
TCP	Tool Center Point

Chapter 1

Introduction

1.1 Context and Motivation

Additive Manufacturing (AM), an advanced manufacturing process, enables the creation of three-dimensional objects by building them layer by layer. This technique utilizes Computer-Aided Design (CAD) data files and is commonly referred to as 3D printing. This technology is commonly used for modelling, prototyping and tooling [1]. Modeling is utilized to explore and refine designs, prototyping is employed to test and validate design concepts, and tooling is used to create necessary tools or moulds for other processes. According to Gibson *et al.* [2] 3D printing presents a wide variety of advantages that support its use, these being related to the materials used in the process, the speed of the fabrication and complexity of the parts to be manufactured. 3D printing can be performed with a wide variety of materials. It grew around polymeric materials, waxes and paper laminates, but nowadays it is possible to print composites, metals and ceramics. With this technology, a part can be manufactured just in a few hours, and it is possible to produce multiple parts simultaneously. The main advantage of this process is the complexity that can be achieved when compared to conventional production methods such as machining. Additive manufacturing processes are not limited in the same way, and parts with more complex features can be fabricated easily without specific planning of the process.

This type of technology can be classified according to the melting system, these being laser, flashing source, jetting or extrusion [1]. This dissertation will focus on the extrusion technology, more specifically the Fused Deposition Modelling (FDM). It consists in the extrusion of a material, normally a thermoplastic, through a nozzle to print one cross section of a part, moving vertically and repeating the process for each layer until it is complete.

3D printing was mainly applied to small parts in the millimeter range. More recently, the need to create ever increasing parts, is creating a relatively new field of research. 3D printing is considered large scale when the printed parts are approximately one cubic metre or larger in volume [3]. This technology has been explored mainly for construction automation using concrete instead of thermoplastics to construct building-sized objects rapidly. The interest in large-scale

printing with thermoplastics comes from real size prototyping and rapid tooling to make moulds, for example, to be used in other manufacturing processes (e.g. thermoforming).

In FDM, since thermoplastic materials are melted and resolidified, the deposited material contracts causing inner stresses on the layer. The types of defects usually associated with this effect are deformation, including warp and inner-layer delaminating or cracking [4]. According to Dezaki *et al.* [5] if the cooling time between deposition of consecutive layers exceeds the optimal time, delamination issues can occur. If the cooling time is not enough material from the bottom layer can drop or wrap while depositing the next layer. As the prints are scaled up in size, deformations due to thermal stresses remain a major obstacle on the process [6]. According to Wang *et al.* [7] the 3D printing technology of large parts is still too challenging to be accepted by the industry. If some error or deformation occurs during the process, the whole operation of printing needs to be suspended which is translated into a waste of materials and time. The implementation of control systems was suggested as a way to overcome this type of inconvenient.

At INEGI, where this master thesis was developed, drop deformations were observed on nearly every FDM print, due to insufficient cooling time between layers. The established project fits in the development of a real-time control of the material deposition during the FDM process of large parts.

1.2 Integration of the Project in INEGI's Framework

INEGI, Institute of Science and Innovation in Mechanical Engineering and Industrial Engineering, aims to contribute to the development of the Portuguese industry and economy through innovation in a scientific and technological basis.

Recently, INEGI acquired an FDM system composed by an industrial KUKA robot and CEAD extruder developed to large-scale 3D printing. The extruder is equipped with a nozzle, that extrudes material with a diameter between 4 mm and 10 mm. This means that the deposited beads (hight x width) can vary between 2 mm x 4 mm and 8 mm x 17 mm. The materials printed using this system are thermoplastics reinforced with fibers. Because of the large dimensions of the beads and the low thermal conductivity of the material, there is a difficulty in cooling down the previously deposited layer before a new one is built. It was consistently observed that most printed parts were deformed during the process. Since the material does not cool down enough for the new layer to be deposited, it gets dragged and drops appear between the layers.

1.3 Objectives of the Project

INEGI proposed a project seeking the optimization of the cooling process for the material during deposition. One of the available equipments to integrate on the robot control was a thermal camera capable of measuring the temperatures distribution over a specified area.

The proposed project involved three main steps. On a first instance, it was necessary to design a support to attach a thermal camera to the robotic arm. Secondly, a software was developed

in order to control the camera and the measurement of the temperature on the areas of interest. Alongside this step, the routines of the robot were modified so that the deposition is controlled according to the data collected.

1.4 Methods Followed in the Project

This masters dissertation started with research on the topic of large-scale 3D printing and the state of the art of thermal optimization during the process.

Following this, some C# programming was developed, specifically how to access the live image of the camera and how to get the values measured by it. Simultaneously, some imaging tests were performed.

A priority in this project was to establish the communications configuration for the system. It was important to develop the main lines of how the system should behave in order to better understand which variables were necessary and which type of connections would happen between the entities.

After the connections were set up, C# programming took place and an implementation of a basic algorithm was established. This first application was tested by simulating the code of the robot and placing a heated object below the camera to test the algorithm. When it was fully working, a second application was developed in order to properly control the system.

To finalize the project, some printing experiments were conducted with the objective of demonstrating the impact of the solution developed.

1.5 Organization of the Document

This document is structured into 8 chapters, each of which presents a distinct phase of the project's development. The **Introduction** (chapter 1) aims to clarify the motivation of this dissertation as well as its main objectives. The **State of the Art** (chapter 2) exposes the advances concerning the thermal optimization of 3D printing processes. In the first place, some literature about the integration of infrared cameras in 3D printing processes is analyzed. Then, some thermal optimization of the deposition in large-scale printing is studied. Chapter 3, **Problem Statement**, presentes the system used and its challenges that served as the impetus for the development of this dissertation. The **Camera Selection and Positioning** (chapter 4) explores the criteria and the obstacles that were overcome in order to attach the thermal camera to the robot. The 5th chapter, **Communication Configuration** clarifies the relation between the entities of the system as well as its intended behavior. It also establishes the communication protocols applied between each device. The **Application Development** (chapter 6) follows the different steps of the camera data processing development. First, the modifications of the robot routines are exposed, then two approaches were considered to process the images acquired. On chapter 7, **Experiments**, the solution was tested and validated. A discussion of the results was conducted in order to compare the previous

system to the modified one. Finally, on **Conclusions and Future Works** (chapter 8), the dissertation is concluded by presenting the main findings of the work and discuss which improvements can be added to the final solution.

Chapter 2

State of the Art

Due to limited research on large-scale 3D printing with thermoplastics, there is a lack of literature regarding the optimization of material deposition in this context [8]. However, there has been a crescent interest in monitoring the layer temperature during FDM processes in order to understand its influence on the final printed parts.

2.1 In situ Monitoring of Layer Temperature During 3D Printing Deposition

Monitoring the layers' temperature during deposition is important to understand the inter-layer bonding since it is intimately related to the quality of printed components [8]. There are some methods that can be utilized in order to get the temperature of the layers during the printing process. The in situ approaches are based on thermocouples and Infrared (IR) cameras [9].

2.1.1 Temperature Monitoring via Thermocouple Integration

Kousiatza and Karalekas [10] embedded Fiber Bragg Grating (FGB) sensors and K-type thermocouples within different layer locations inside test specimens. The sensors were placed in order to ensure sufficient contact with the material being deposited.

Yin *et al.* [11] and Vanaei *et al.* [12] used K-type thermocouples to measure the temperature of the different layers. While Yin *et al.* [11] placed a thermocouple every time a layer was deposited, interrupting the process and restarting it after, Vanaei *et al.* [12] incopored a sensor every 5 mm in height without stopping the printing process. A similar approach was explored by Xu *et al.* [13] with T-type thermocouples. The sensors were introduced during a FDM process pause of 8 seconds every 5mm of height of the print. The principle utilized on this type of method is ilustrated on Figure 2.1.

The termocouple method has not been really explored on large-scale thermoplastic FDM processes since security barriers normally isolate the large-scale printing system. The application of

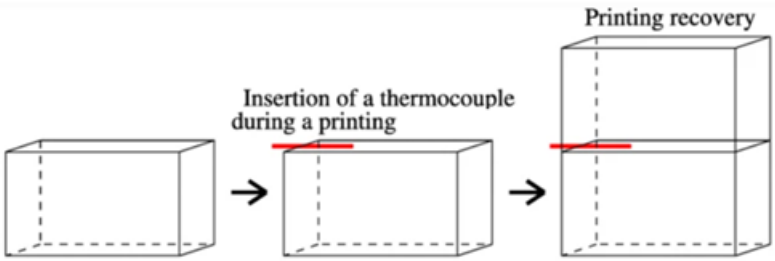

Figure 2.1: Placement of thermocouple between layers

thermocouples on this field was only documented by Caltanissetta *et al.* [14] and the sensors were placed on the extruder nozzle in order to monitor the extrusion temperature. On the same study, for the layer temperature monitoring, an IR camera was used so this topic is explored on Section 2.1.2.

2.1.2 Temperature Monitoring via Infrared Cameras

IR cameras were utilized by Seppala and Migler [15] in order to study the temperature profile on a FDM process, focusing on the inter-layer region. Measure the temperatures accurately allows the understanding of the weld between the layers. To achieve this objective, a camera was used and placed in front of the build volume, centered on the printed object with the extruding layer in the center of the frame as observed in figure 2.2.

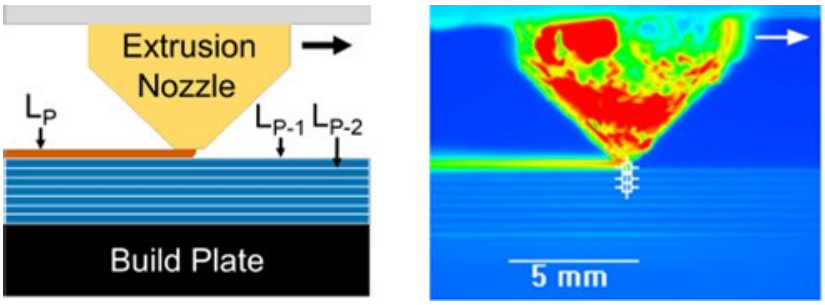

Figure 2.2: Position of the IR camera as an illustration (left) and real image (right) [15]

Instead of using the camera image directly, Seppala and Migler [15], analyzed the raw camera output. Some non-uniformity corrections were necessary in order to get good quality data. It was also necessary to remove the reflections and determine the relationship between the camera signal and the temperature. Concerning the camera's Region Of Interest (ROI) , it was selected in such way that the layer boundary is normal to the camera. Lastly, it was concluded that the application of IR thermography should be explored in the future so that the thermoplastic extrusion processes can be improved.

Similarly, Ferraris *et al.* [16] and Lepoivre *et al.* [17] also studied the inter-layer adhesion through an IR camera application. These projects did not delve as deeply into the monitoring process as Seppala and Miggler [15] since the final objective was to compare the results to numerical models.

Concerning the large-scale temperature monitoring, Dinwiddie *et al.* [18] printed hexagon shaped parts of different sizes in Acrylonitrile Butadiene Stryrene (ABS) while measuring the temperature using a Flir A35 thermal camera. In this study, the camera was attached to the moving part of the printer as shown on Figure 2.3 , 42 cm from the required view and the images were taken at a 30 Hz rate.

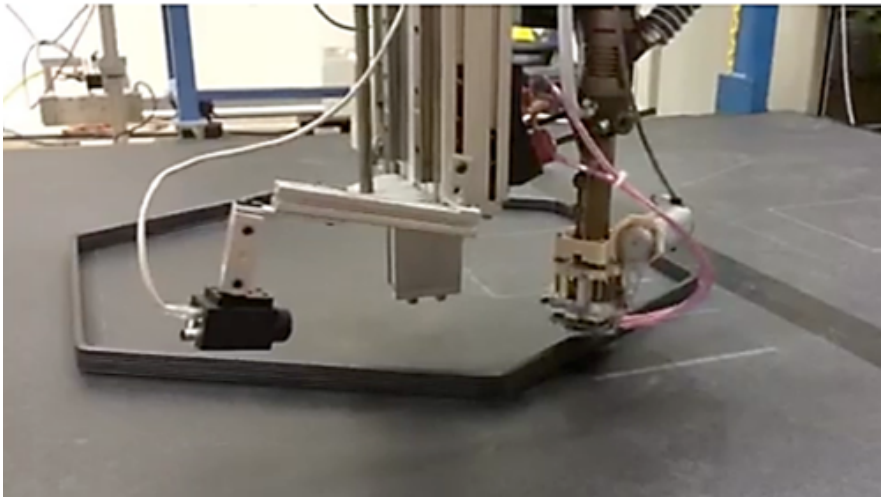

Figure 2.3: Camera setup utilized during the experiment [18]

As expected, as the hexagon and travel time got bigger, the temperature of the previous layer lower significantly. On a hexagon with a side of 43 cm, the previous layer was at 172 °C while in the hexagon with a side of 173 cm the previous layer was at 110 °C. Dinwiddie *et al.* [18] also concluded that materials reinforced with carbon fiber increase the extrusion temperature and maintain the deposited layer hot for a longer time.

Compton *et al.* [6] also preformed a thermal analysis of large-scale thermoplastic FDM process. The experiment consisted in printing a wall (0.02 m width and 0.35 m height) in ABS reinforced with 20% carbon fiber. A Flir A35 thermal camera was positioned 1.2 m from the central position of the wall in order to observe the full wall height as shown in Figure 2.4 . A video was captured during the process with a frame rate of 1/s.

Through the camera software the temperature data was exported and then compared to a numerical model. It was concluded that the temperature of the top layer just before deposition of a new one could be considered as indicator for the degree of wrapping and cracking. The temperature of the top layer must be kept above the glass transition temperature of the material in order to prevent delamination of the part. Also, the higher the thermal conductivity of the material, the harder it is to scale-up on the part to be printed.

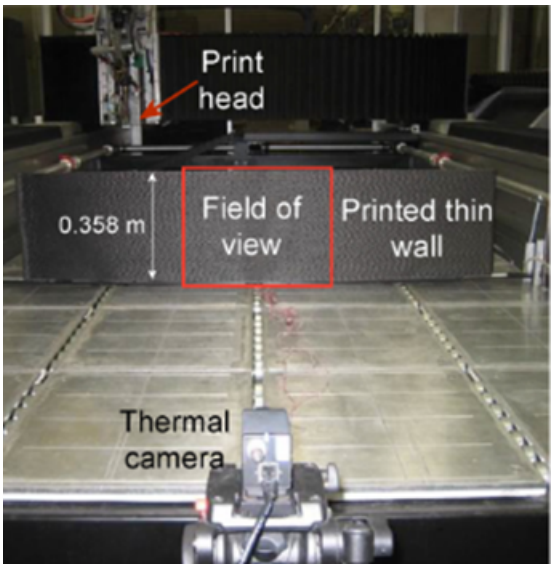

Figure 2.4: Camera setup utilized during the print [6]

More recently, Caltanissetta *et al.* [14] developed another similar solution for real time temperature monitoring of material extrusion processes. In Caltanissetta study, the material used was also ABS reinforced with 20% carbon fiber. For the toolpath, a connected serpentine trajectory was defined with five long beads (650 mm) that are connected to one another with short beads (25 mm) as shown in Figure 2.5. 20 layers were deposited each with 2 mm of height.

Figure 2.5: Serpentine printed during the experiment [14]

During the operation, using a Flir A35 thermal camera, IR videos were acquired. The camera was positioned 1.3 m from the target object and with a 45° inclination taking as reference the building platform as shown in Figure 2.6. It was fixed to the Z axis of the printer so that the top layer is always visible in the same position within the frames.

The acquisition frequency of the video was 30 fps. The temperature data was exported through the camera software and then post-processed using MATLAB. In Caltanissetta study, two types of analysis were performed. The first aimed to capture and model thermal profiles across different

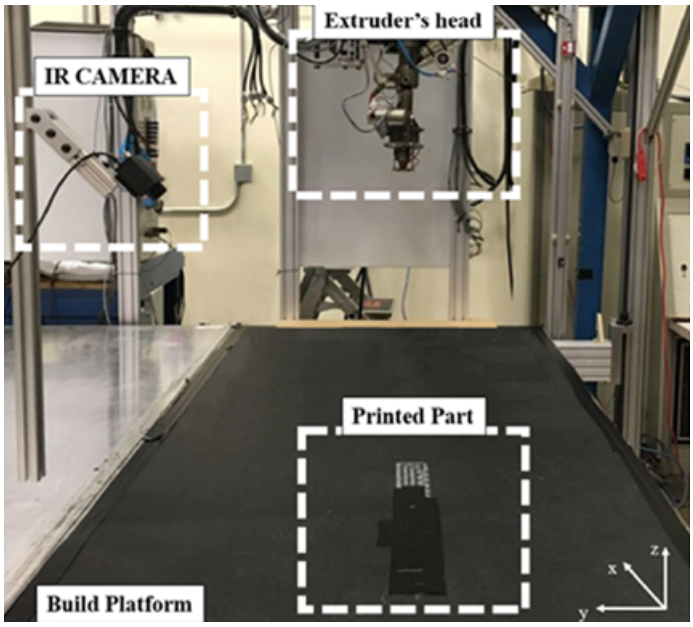

Figure 2.6: Camera setup utilized during the experiment [14]

layers and study its evolution while the other was developed for hot and cold detection. It was concluded that the machine setup and data acquisition can be improved in order to enhance the accuracy.

2.2 Thermal Optimization of the Deposition in Thermoplastic Large-Scale 3D Printing

Concerning the thermal optimization of large-scale printing, minimal documentation was discovered. Borish *et al*. [19] performed hardware and software modifications on a large-scale thermoplastic 3D printer in order to guarantee the quality of the parts printed. From the hardware perspective, a thermal camera was attached to a pneumatic arm (Figure 2.7) of the printing machine.

Figure 2.7: Camera setup on the pneumatic arm [19]

On Figure 2.8 it is possible to observe the printer utilized by Borish *et al*. [19]. A heated bed covered in build sheets of ABS was used to promote the better adhesion of the first layer of the

material.

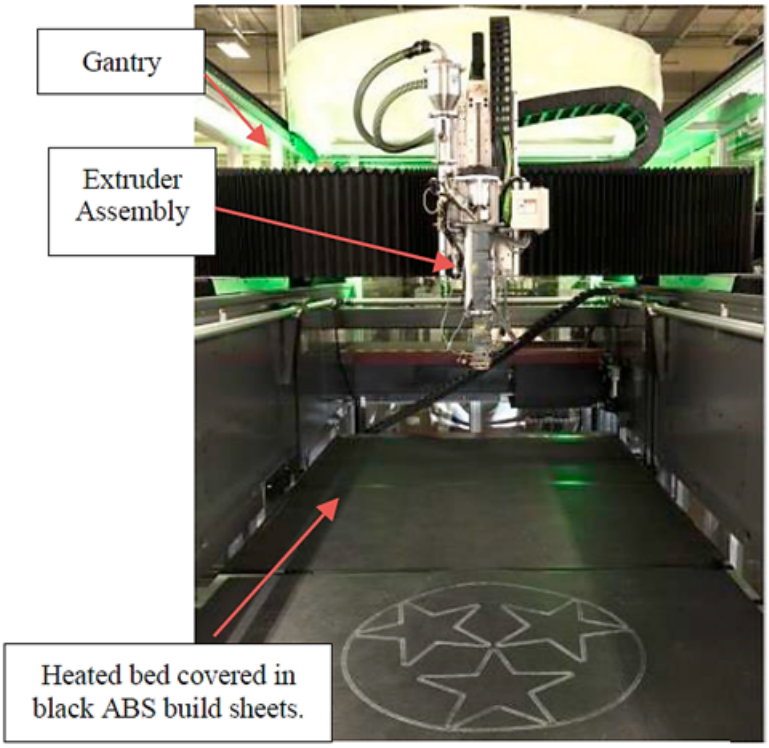

Figure 2.8: Printing machine utilized during the experiment [19]

Regarding the software, some alterations were implemented on the G-code and an appropriate image analysis software was developed. The working principle of the experiment was to calculate the paths of the extrusion tool and camera arm. After a certain number of layers, the printing stops and the camera arm extends in order to measure the temperature. For this, the foreground was identified and its pixels were converted to temperature in degrees Celsius. Only when the average temperature of the layer reaches a desired value, the camera retracts and the printing process continues. The camera recorded data at 1 fps and once the data is collected, an analysis occurs in discrete steps every 10 seconds.

In order to verify the efficiency of the modifications to the printing machine, an object was printed with a 20% carbon fiber reinforced ABS with and without the modifications implemented. On Figure 2.9 it is possible to observe a failed printed object (on the left) due to excessive heat on the layers during the process and a successful printed object (on the right) after implementing the modifications in the system.

The object on the left failed to print after 12 minutes into the process. In this case, the walls were too hot to support the weight of the upcoming layers which caused them to collapse. The printed object on the right was built as intended after a waiting time between layers was employed. These modifications allowed the material to solidify enough and gain the necessary rigidity to support its own weight.

Although the thermal related deformations were solved, two major drawbacks were identified: overall build time and material waste.

Figure 2.9: Failed print object (left) and successful print object (right) [19]

Considering a solution based on waiting times, the overall build time can increase significantly [19]. On the object of Figure 2.9, the printing time without the waiting time was expected to take two hours, while the printing time of the object with the waiting time took eleven hours. The average waiting time between layers was approximately 4 minutes so that the temperature dropped from 210°C to 115°C for the process to continue. Nevertheless, most objects are unlikely to experience such a significant increase in build time. The experiment was performed on a relatively small box which caused the majority of the time to be waiting time. A typical large-scale object is made of layers that are a combination of shorter and longer paths which results in a range of layer times. That means that only specific layers would require longer waiting times while others might need no time at all.

The surface quality of the objects printed may present some issues due to the material that lays in the nozzle while the waiting time goes on. This material, when extruded on the next layer, presents an inferior surface quality when compared to the material that is deposited continuously. In order to prevent these issues, the laying material is removed before the next layer is deposited with the objective of building the object with a better quality material. Material wastage can be a consequence of this method, although it could be solved by implementing a flow control system.

Summarizing, there is a crescent interest in understanding how the temperature can influence the bonding between layers in 3D printing processes [8]. The IR cameras are recurrently used on this type of analysis since they can provide data in real time. Even though the large-scale 3D printing processes are recognized as a powerful method for prototyping and rapid tooling [1], there are still many difficulties associated. And because this technology is recent, there is not much literature concerning the thermal optimization of the process [8]. Given that information and considering the experiments mentioned, on this project it was expected that deformations due to excessive heat during printing would be eliminated [19]. It was anticipated a longer build time and material waste which are downsides of the thermal optimization through implementation of waiting times between layers.

Chapter 3

Problem Statement

In this chapter, the project's system and its components as well as its working principle are presented. Afterwards, the 3D printing process is explained from the part design until the final product is manufactured at INEGI. Finally, a review of the system is performed and the problem is stated.

3.1 System Presentation

On figure 3.1 it is possible to observe the system around which the project was developed.

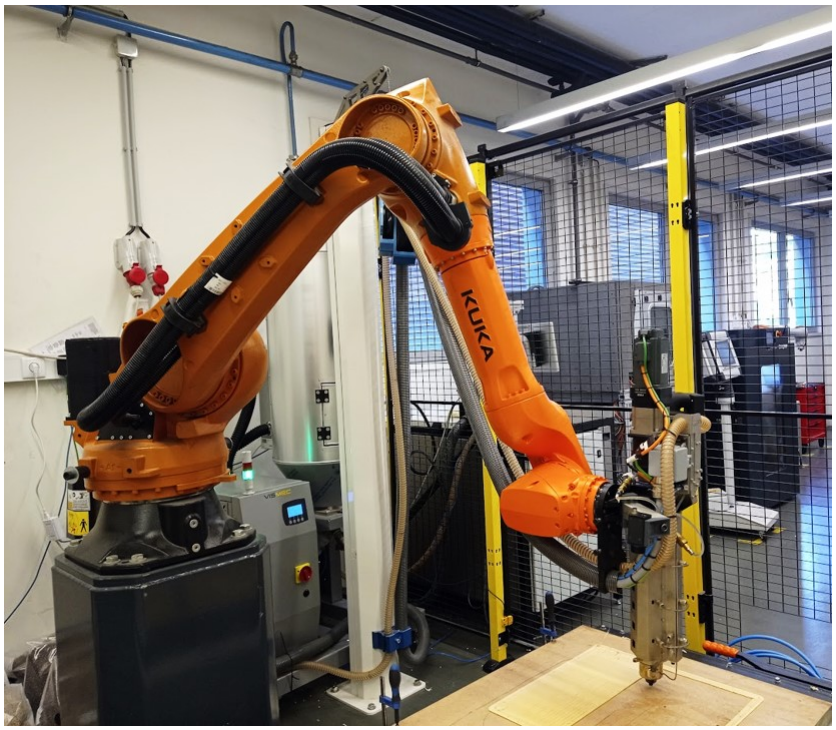

Figure 3.1: Robotic cell for 3D printing at INEGI

The system is composed by two subsystems. One of them is a 6-axes industrial KUKA robot (KR50R2100) and its controller (KR C4). The other one is a screw and barrel CEAD extruder developed to deposit thermoplastic materials with nozzles specifically designed for 3D printing. The robot (Appendix A) is responsible for controlling the movements according to a predefined code and adapts the speed of the extrusion screw to it. The extrusion system (Appendix B) also has a controller that is responsible for: the material feeding, maintaining the temperatures at the different zones stable and controlling the motor responsible for the movement of the extrusion screw according to the robots' set-points.

In a more detailed view the extruder has four heating zones and one cooling zone (water cooled). The heating control is preformed by a Siemens PID controller. Also, on the available CEAD software touchscreen it is possible to monitor all heating zones temperatures, turn on and off the transport of material, heaters and extrusion. It is also possible to visualize the speed of extrusion screw in RPM and adjust some configurations. These features are visible on figure 3.2.

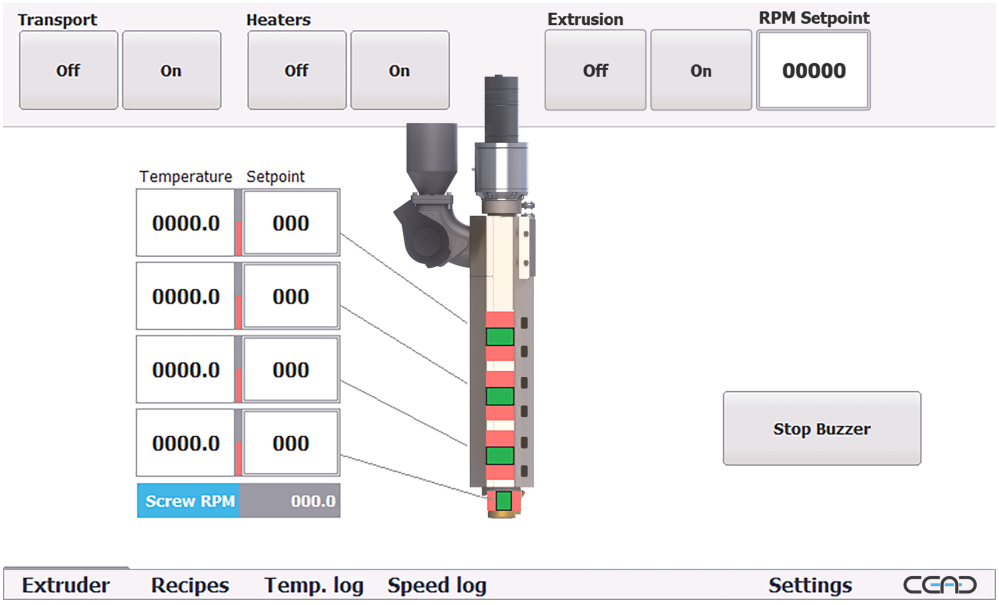

Figure 3.2: CEAD extruder control panel

3.2 3D Printing Methodology at INEGI

In order to print an object through a FDM process it is necessary to follow a set of steps, such as: design the object to be manufactured, slice it so that the layers are created and the trajectory of the tool is defined, export the code to the robot controller. On figure 3.3 it is possible to observe the 3D printing methodology at INEGI.

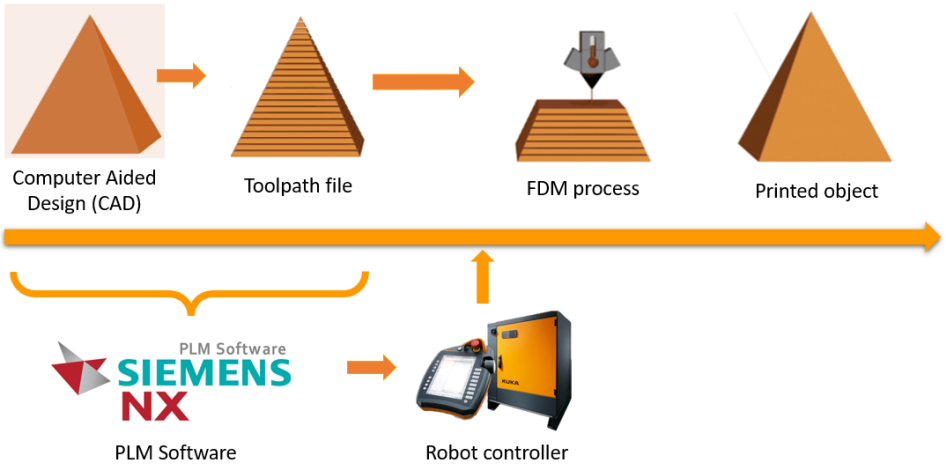

Figure 3.3: FDM metodology at INEGI

After the object is modeled, it is sliced, which means that the tool path is calculated and converted to the robot language, KRL. Then, it is simulated to check for possible errors. The software used for these steps is the Siemens NX, in addition to enabling object modeling and tool path calculation, it also incorporates the robotic cell from INEGI, allowing for simulation and conversion of G-code language. Lastly, the final code is exported to the robot controller and through the *SmartPAD* it is possible to execute it. The robot perfomrs the defined trajectory and the material is extruded as intended until the object is built.

3.3 Review of the FDM Process

At INEGI, the objects that were printed with this system presented issues during the printing process due to insufficient cooling time of the deposited layers. Deformations were generated when previously deposited material was dragged while depositing a new layer and, also as the object is built up the walls can not handle the weight of the material which makes it collapse.

There were some attempts of minimizing this type of issue through external ventilation. In a first instance, cooling fans were placed around the part that is being printed, however the cooling effect would conflict with the extruder controller. Since the tool's temperature is controlled by its own controller and it is set to a certain value, the cooling would not make it possible for the extruder to reach the extrusion temperature. This created a problem since extrusion would not occur because the tool would never reach the defined temperature. As the external ventilation would introduce another problem a new approach was considered.

The solution implemented more recently includes waiting times without knowing the deposited layer temperature. For a couple of minutes the system would stop depositing material and it would wait a certain time for the material to solidify between layers. As good as it seems, there was no predefined criteria for the application of the waiting time. So, the build could take longer than it would be necessary or not waiting enough time to ensure quality objects.

In order to solve this problem, it was proposed that an available thermal camera could be incorporated to improve the current solution. This way, the waiting time can be based on the temperature read at the moment and the extrusion can be optimized.

Chapter 4

Camera Selection and Positioning

This section is divided into three subsections: Camera selection, Support design and manufacture and Robot calibration. Since there were two available cameras to integrate the project, the first sub-section is devoted to presenting both cameras and selecting the most suitable option for the project. The second sub-section, presents the design process and manufacture of the camera support so that it can be fixed to the robotic arm. In the last sub-section, the calibration of the robot was explored, accordingly to the position of the camera.

4.1 Camera Selection

Since there were two thermal cameras available: Flir A35 and Flir A65, it was necessary to select the one that was most suitable for the project. On Table 4.1 it is possible to observe some of the specifications of both devices.

Table 4.1: Specifications for Flir A35 and Flir A65 cameras

Imaging and optical data	Flir A65	Flir A35
IR Resolution	640 x 512 pixels	320 x 256 pixels
Field of view (FOV)	25° x 20°	48° x 39°
Focal length	25 mm	9 mm
Image frequency	30 Hz	60 Hz
Temperature range	-40 to +550 °C	-40 to +550°C

Considering that the camera is attached to the robot, the most important factor to take into consideration was the distance required by each device to capture the same FOV. The distance from the extruder's top, where the support would be positioned, to the printing table, when the nozzle is 10 mm up, is approximately 500 mm. From that distance, due to its FOV, the Flir A35 captures an image that is 445 mm x 354 mm. To capture the same FOV with Flir A65 a bigger distance would be required. Considering its FOV, the Flir A65 to capture a similar image to the

Flir A35, the camera had to be placed 1 meter away from printing table. This means that the robot would have to be placed much higher so that the camera is capable of acquiring the same data. Using the Flir A35, minor vertical movements would be required. For this reason, Flir A35 was selected instead of Flir A65. In Appendix C, the specification sheet of the selected camera is presented.

After the camera was selected, it was important to explore the options of its positioning relatively to the robot considering the dimensions of the camera and the type of fixation shown in Figure 4.1.

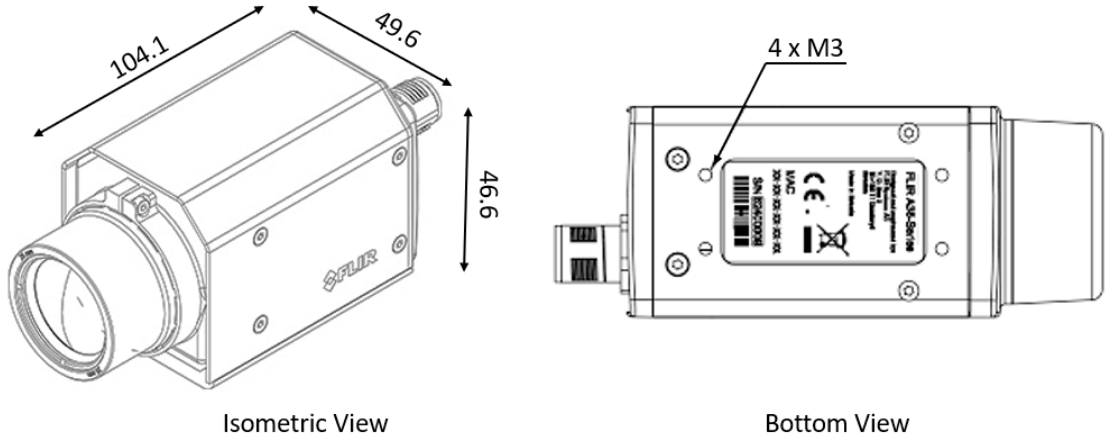

Figure 4.1: Important dimensions considered on support design

4.2 Design and Manufacture of the Camera Support

To conceive a thermal camera support it was necessary to consider its angle of view and position relative to the system. Concerning the angle of visualization, it should be optimized to get the temperature of the last deposited layer, so a top view was preferred. For the position, it was considered that the focus plane should be below the nozzle to ensure that it would not collide with the object being built. Keeping that in mind, some options were developed around a CAD file of the extruder taking advantage of a free triangular shaped portion showed in Figure 4.2.

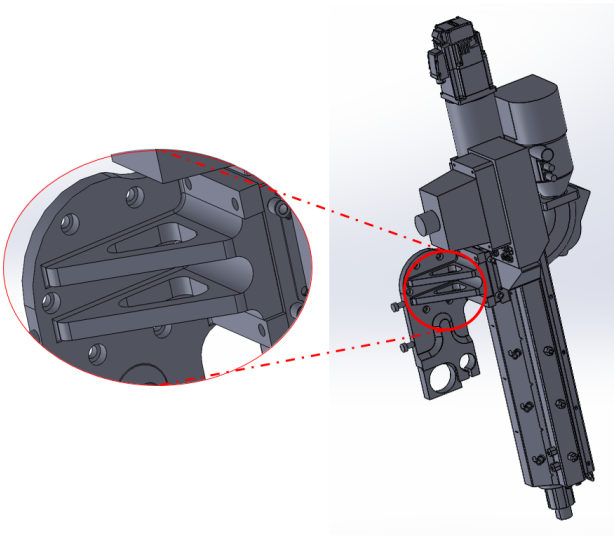

Figure 4.2: CAD file of the extruder and the triangular portion detailed

Initially, it was proposed an aluminium profile based solution, due to its light weight, as shown in Figure 4.3.

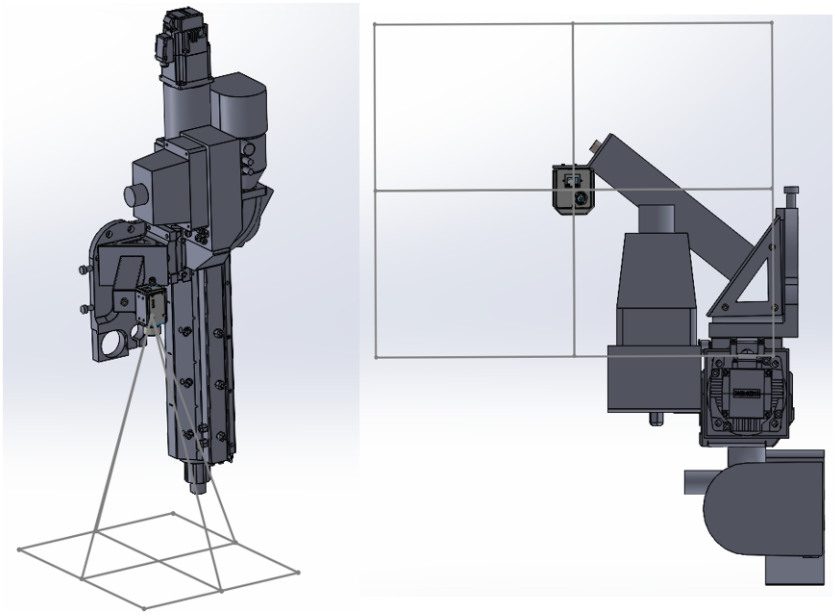

Figure 4.3: First proposal for the camera support

In this solution, a bent aluminium plate was screwed to the triangular shaped portion. To this plate, was also screwed, through a t-connector, a 40 x 40 mm aluminium profile. To mount the thermal camera to the profile, a 135º bent aluminium plate would be secured to the profile and the camera fixed on the other plate's face. The camera's field of view is represented on the image by the straight lines that appear to come out of the lens.

There were some issues associated to this proposal. Firstly, there is a significant amount of cables around the tool, so it is more safe to fix the camera to the other side instead of the proposed

one. Secondly, to secure the aluminium plate it would be necessary to drill three holes on the extruder, which should be avoided. Finally, the part that secures the camera could be not strong enough taking into account the camera weight.

In order to improve the previous approach a simpler solution was developed, as shown in Figure 4.4.

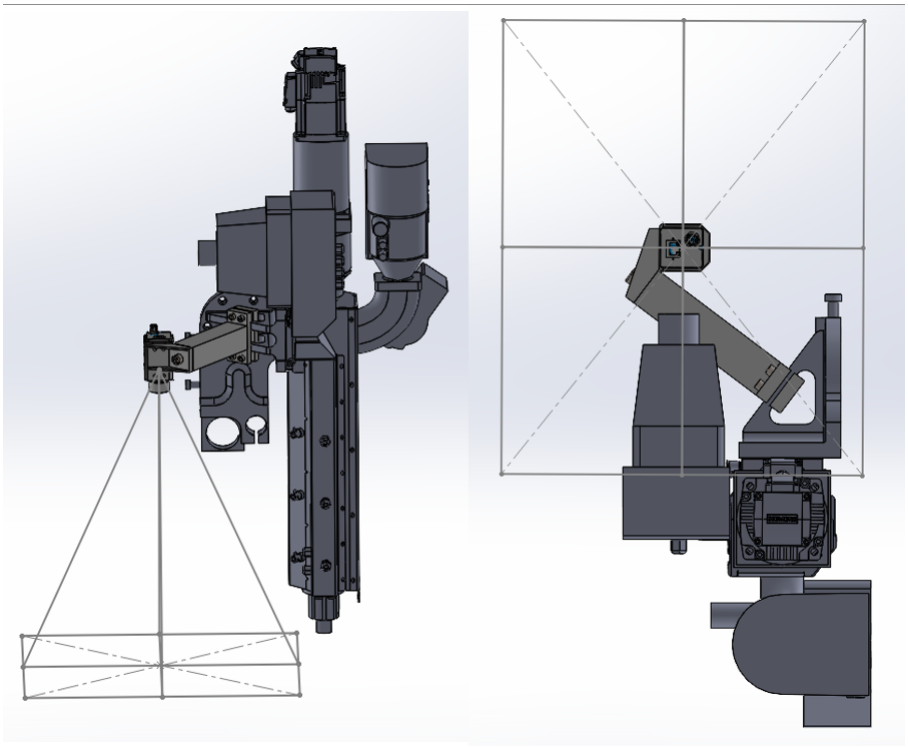

Figure 4.4: Final proposal for the camera support

In this solution, a 40 x 40 mm aluminium profile with 150 mm is used. The camera is oriented differently in order to avoid possible interference between the image and the cables. The parts connecting the triangular shape and the camera to the profile were redesigned so this way it is not necessary to drill the tool. Now, two parts are pressed against the triangular shape in order to keep the support in place. The part that fixes the camera was reinforced to make sure that the camera is secured. Moreover, since INEGI does not possess the required machines to transform the aluminum plate, instead of aluminium, it was decided that it could be printed on the 3D printers available with ABS as the material. This option also reduces the weight of the overall support. Appendix D presents the dimensional drawings for the connecting parts and an exploded view drawing, including the list of materials, of the entire support. Figure 4.5 shows the 3D printed parts that constitute the support.

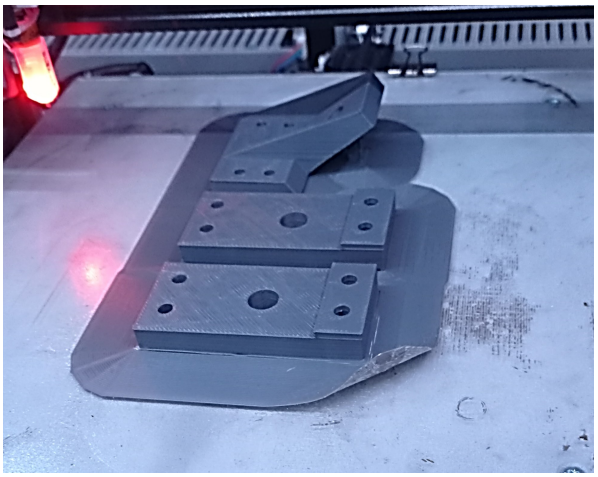

Figure 4.5: Printed connecting parts of the support

The fabricated support is shown on Figure 4.6.

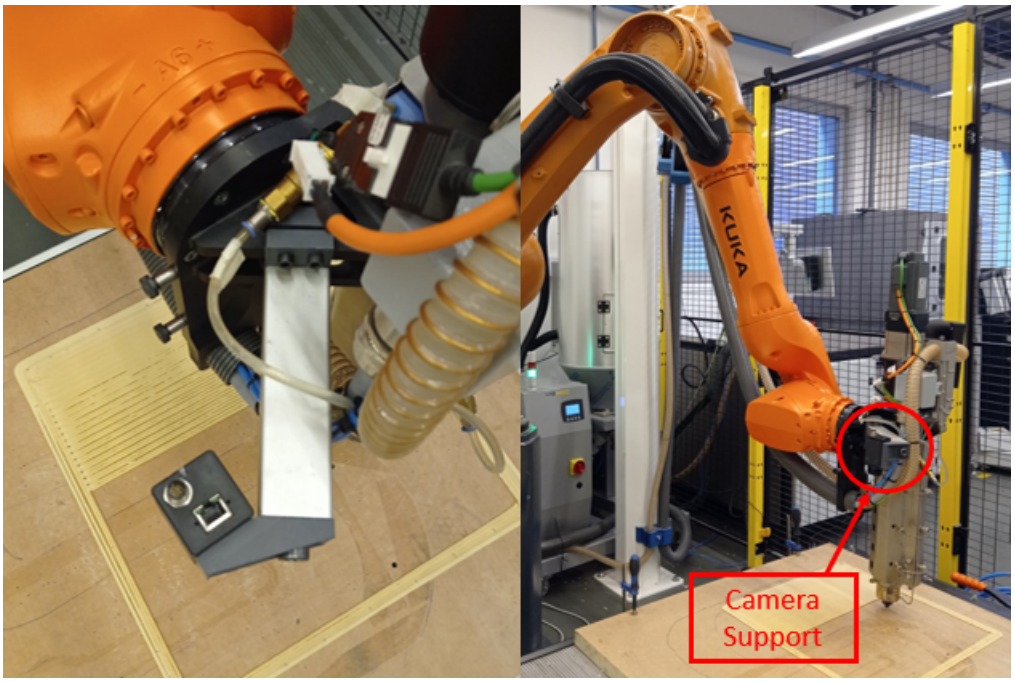

Figure 4.6: Camera support attached to the robot and its location

After the support was attached to the printing system it was important to calibrate the robot in order to capture good quality data.

4.3 Robot Calibration

The attachment of the camera to the robot, means that the camera position depends on the robot's position. For this reason, it was necessary to define the camera as a robot tool.

To define a tool it is necessary to teach the robot at least 4 positions around a point of reference [20], this one being the Tool Center Point (TCP) as shown in Figure 4.7.

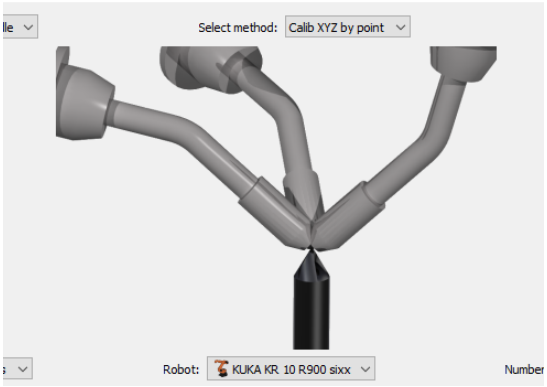

Figure 4.7: Tool definition using 4 positions [20]

The positions are reached by jogging the robot the closest possible to the TCP from different orientations. However, defining the camera as a tool has to follow a slightly different method.

The distance from the camera sensor to the tip of the nozzle of the extruder is about 500 mm, so the idea was to focus the camera for that distance and then using an image capturing program and a soldering iron trying to center the hot point. The setup for this task is shown in Figure 4.8.

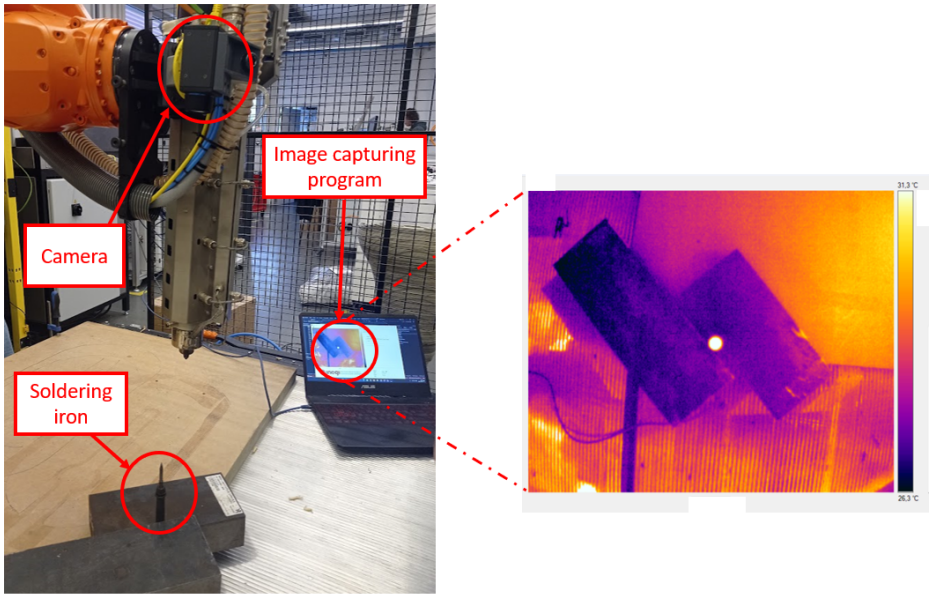

Figure 4.8: Tool definition setup and captured image

On the captured image is noticeable the tip of the heated soldering iron. While jogging the robot in different positions to focus on the soldering iron point it was also measured its distance to the camera to verify if the 500 mm were respected. After capturing 4 different positions focusing on the reference point, the robot controller did not accepted the points since the error between

positions was higher than 5 mm. The procedure was repeated but with no success. So another method had to be tested.

Holding the soldering iron, there were some iron blocks with very prominent corners as shown in Figure 4.8. So the previous method was adapted to the block's corner. Instead of trying to center the tip of the soldering iron, the corner of the block was centered and then measured its distance to the camera. This time, the robot's controller calculated an error inferior to 5 mm which means that the camera was successfully defined as a tool.

Chapter 5

Communications Configuration

Once the camera and the robot were attached, it was necessary to establish how these two devices will work together to enhance the 3D printing process. In this chapter, it is explained the interaction between the devices in the system and the type of communication protocols that were implemented.

5.1 System behavior

The system is composed by the robot, extruder and thermal camera. In order to process the images captured by the camera and establish control over the robot's positioning during printing, it was necessary to develop an application. Chapter 6 explores the application development and image processing algorithm. For now, only the interaction between the robot and the application were explored.

For the connection between the robot system and the application to be possible, some interface it is needed to exchange data between the two devices. At INEGI, there is a *Beckhoff* control panel in which a *TwinCAT* PLC is continuously running in order to exchange data with the robot. Using the *TwinCAT* PLC it is possible to transfer data between the robot and the application. Keeping this in mind, on Figures 5.1 and 5.2 are represented the robot's grafcet and the application's grafcet, respectively.

The goal is to modify the robot's program by adding after each layer a command for it to stop printing and position the camera on the center of the deposited layer. When the camera is positioned properly the robot changes the state of a variable, so that the application starts the image processing. The image processing consists in constant evaluation of the temperature of the points of interest and it will be explored on Chapter 6. When those points reach a previously defined value, the application changes the state of another variable letting the robot's program to continue its operation.

Considering that the system would behave accordingly to what was previously mentioned, it was necessary to define the communication protocols between the different entities.

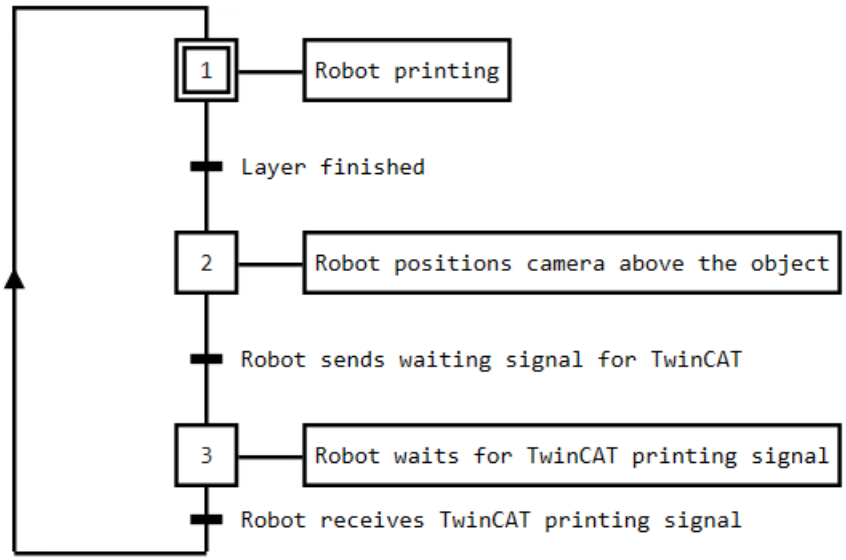

Figure 5.1: Robot behavior grafcet

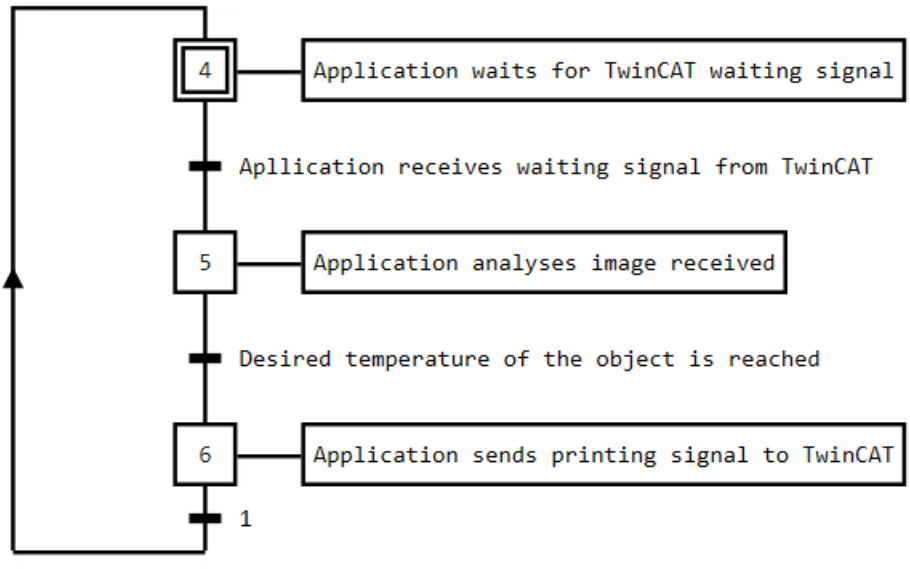

Figure 5.2: Application grafcet

5.2 Communication Protocols

The scheme of the Figure 5.3 demonstrates the communication protocols that were implemented in order to develop the project.

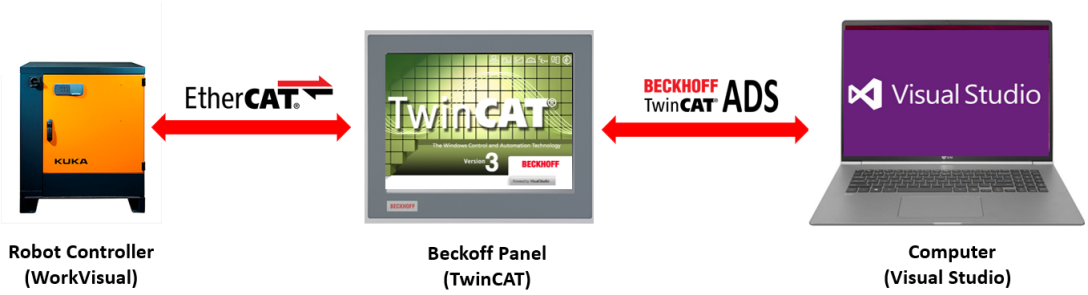

Figure 5.3: Communication protocols between systems

There were three main entities that are involved on this project: the robot controller, a *TwinCAT* PLC responsible for data exchange and a computer to run the application. The WorkVisual software makes it possible to configure the robot controller using projects and databases. There is a robot's project in which variables of interest are selected and connected to an *EtherCAT* bridge. The variables from the robot are connected to this interface which is also connected to *TwinCAT*. The communication protocol used is called *EtherCAT* Automation Protocol (EAP) and will be explored in the Section 5.2.1. This technology was previously implemented on the system by INEGI in order to access robots data, as previously mentioned. In this project, it was only necessary to define more variables related to the process control.

The communication between the *TwinCAT* and the application (Visual Studio project) was performed by Automation Device Specification (ADS) that is a communication protocol that will be explore in the Section 5.2.2.

5.2.1 *EtherCAT* Automation Protocol

EtherCAT was developed by *Beckhoff* and it is a real-time industrial Ethernet technology. Traditionally, it is based on master/slave architecture, a master device sends, for instance, a data frame, that passes through each node and the slave devices read the data addressed to them and insert its data, if requested, in the frame as it is moving downstream [21] as shown in figure 5.4.

On top of this technology, EAP was developed to be used as a general protocol to exchange data between controllers (master/master communications) or interfacing with a central master computer [22].

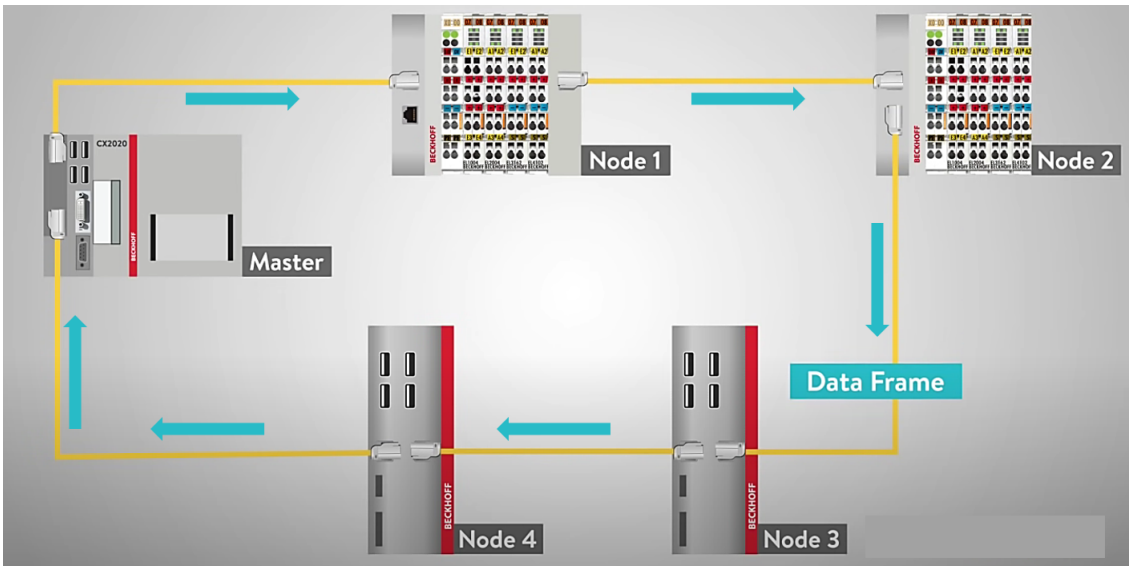

Figure 5.4: Working principle of *EtherCAT*

At INEGI, the *EtherCAT* connection was established between the robot and the *TwinCAT* PLC through a *EtherCAT* bridge as shown in Figure 5.5.

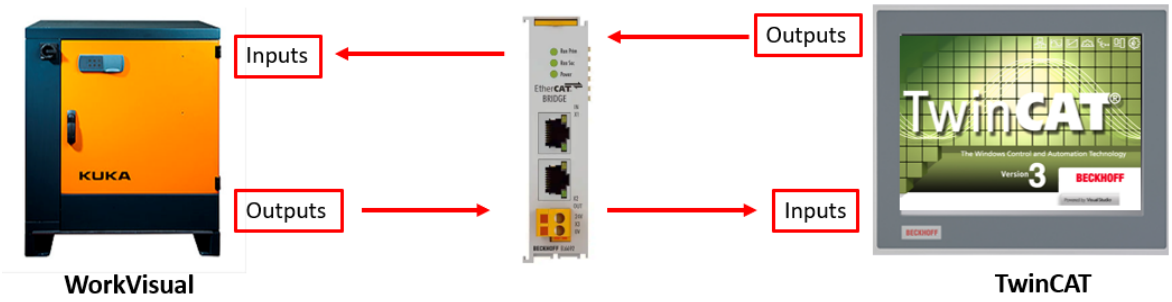

Figure 5.5: Connection between WorkVisual and *TwinCAT*

The *EtherCAT* bridge was configured in WorkVisual (and uploaded to the robot's controller), and also in *TwinCAT*. The output data from the robot controller is connected to the bridge, so it can be read by the *TwinCAT*. It is also possible for the *TwinCAT* to change the variables state or value, once the outputs of the *TwinCAT* are connected to interface as well.

Table 5.1 presentes the main variables that are exchanged between the WorkVisual and *TwinCAT* before the implementation of the thermal optimization solution.

Table 5.1: Exchanged variables between the robot and *TwinCAT* before the process optimization

Variable Name	Variable Type	Description	Robot I/O	*TwinCAT* I/O
PosAn	Real	Position of joint n*	Output	Input
TempAn	Real	Temperature of joint n*	Output	Input
Posm	Real	Relative position and orientation of TCP in m**	Output	Input
RPM_vol	Real	Extrusion speed in RPM	Output	Input
FuncStat	Integer	Operation mode of the robot	Output	Input
TGrain	Boolean	State ON/OFF of pellet transportation	Output	Input
Ext_Lig	Boolean	State ON/OFF of the extrusion	Output	Input

* n is an integer number between 1 and 6 representing the robot's joints.

** m assumes X,Y,Z,A,B and C letters and represent the TCP position and orientation.

Until this project has began there was no interest by INEGI to send data to the robot's controller since the goal was only to know the state of the robot. However, in this project, by analysing the intended system behavior , it was necessary to define three more control variables. These are presented on Table 5.2.

Table 5.2: New defined variables between the robot and *TwinCAT* for the process optimization

Variable Name	Variable Type	Description	Robot I/O	*TwinCAT* I/O
robot_wait	Boolean	The robot finished the layer and the camera is already positioned to acquire data	Output	Input
robot_print	Boolean	The layer has reached an acceptable temperature to continue the process	Input	Output
cam_connected	Boolean	The application is running	Input	Output

As referred in Section 5.1 some coordination between the robot and the application was required. When the robot starts executing its program, the variable "robot_wait" is set to "false". At the same time, the application is also executed and, the variable "robot_print" is set to "false" while the "cam_connected" is set to "true".When a layer is finished by the robot, it positions itself so that the camera is above the deposited layer. Afterwards, it changes the variable "robot_wait" to "true". When the application detects that the "robot_wait" is set to "true" the temperature of the layer is evaluated. And, when it reaches an acceptable value, it sets the variable "robot_print" to "true". At this point, the robot continues to print the next layer, and the variables "robot_wait" and "robot_print" are set to "false".

To define these new variables it was necessary to modify the *EtherCAT* bridge configuration on WorkVisual and on the *TwinCAT* PLC. On both, the I/O interfaces were connected to the *EtherCAT* bridge as shown on Figure 5.5. On Figures 5.6 and 5.7 it is possible to observe how each variable was defined in WorkVisual and *TwinCAT*, respectively.

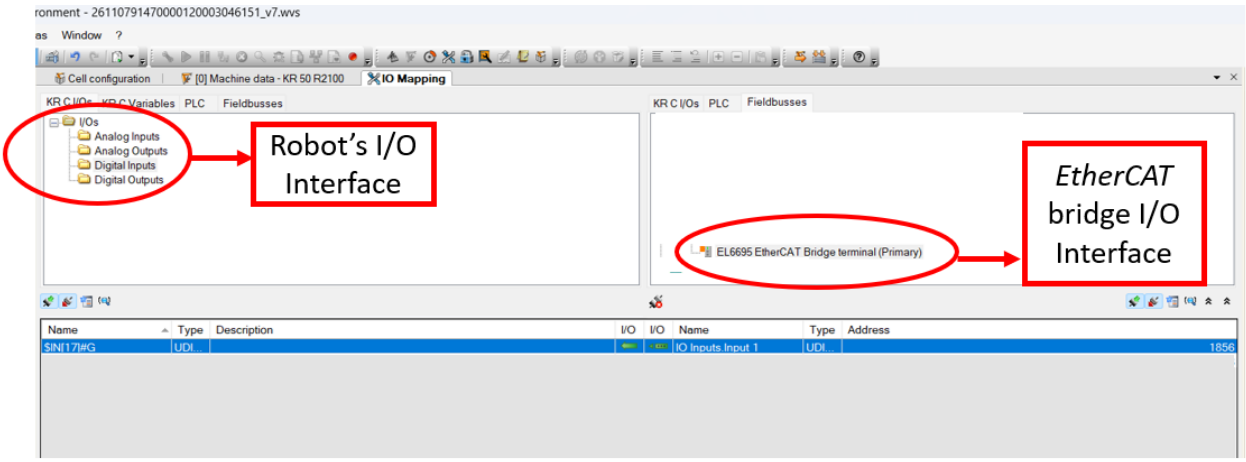

Figure 5.6: I/O Interface connection between the robot and the bridge

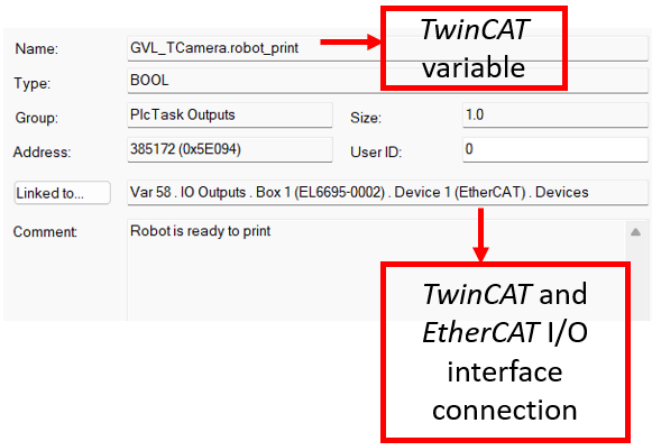

Figure 5.7: I/O Interface connection between *TwinCAT* and the bridge

Summarizing, the communication was successfully implemented between the two entities, so that it was possible to exchange data between the robot controller and the *TwinCAT* PLC. The next section explores the ADS protocol and how it was performed so it was possible for the application to communicate easily to the *TwinCAT* PLC.

5.2.2 Automation Device Specification Protocol

According to *Beckhoff* [23], the ADS protocol allows the communication between different software modules from any point within the *TwinCAT* system. This technology runs on top of TCP/IP

protocols which is used to link network devices on the internet. At INEGI, the connection between the different devices is represented on figure 5.8.

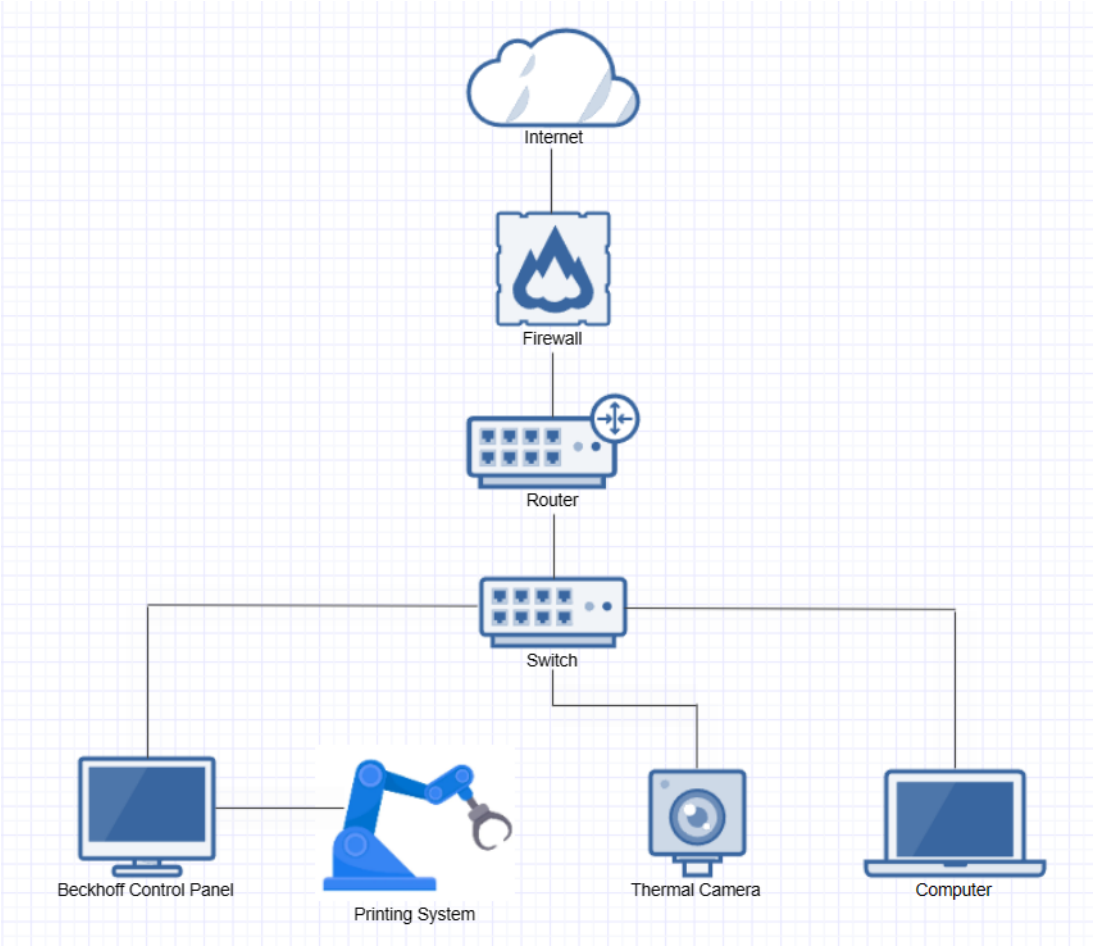

Figure 5.8: Network diagram of the project's devices

To the same network are connected: the *Beckhoff* Control Panel in which the *TwinCAT* PLC is running, the printing system, the thermal camera and the computer where the application is executed. This connection enables the ADS communication between the the application and the *TwinCAT* PLC.

To establish the communication, segments of code were inserted in the application indicating the port that is being accessed, which variable is being targeted and if the goal is to read the value or to write the value on *TwinCAT* [24]. Considering the intended system behavior , when the robot program starts, the application also starts and it sets in *TwinCAT* the variable "cam_connected" to "true". When the robot sets the variable "robot_wait" to "true", indicating that the camera is positioned correctly, the application starts the image processing. So, it is required by the application to continuously read the variable and begin the processing when it is set to "true". When the processing is finished, the application sets the variable "robot_print" to "true" making the robot continue the printing. At this point, the robot sets the variable "robot_wait" to "false" and the application sets the variable "robot_ print" to false. This is repeated for all layers until the object is concluded.

On Figure 5.9 is shown an example of communication using ADS.

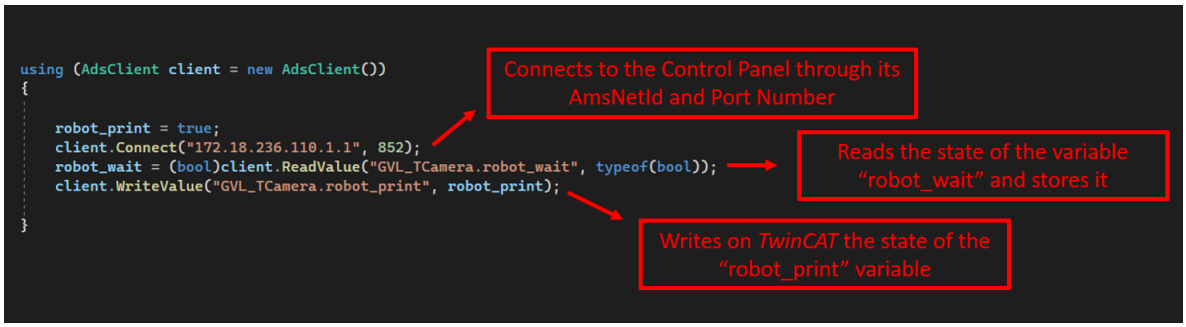

Figure 5.9: Example of communication using ADS between a Visual Studio Project and *TwinCAT*

After ensuring the successful functionality of all communication protocols, the next step was to develop the application to acquire the camera's data and process it as it is explored on the next Chapter 6.

Chapter 6

Application Development

In this chapter, the development of the application and the implemented algorithms are explored in order to create a solid solution for the problem. The first section is dedicated to the method of modification of the robot's KRL program that contains the instructions of movement and extrusion which was crucial for the application development.

Concerning the application, two approaches were considered: the first one is simpler since the points of interest are not defined by the object itself but by a temperature threshold, and the second one is a bit more complex and takes into account only the points that belong to the part being built. For both approaches the application was programmed in C#. Each approach section is divided in four sub-sections: Relevant Considerations, HMI Design, Image Processing Algorithm and Problems and Improvements. Initially, everything that was taken into account for the solution is exposed. Afterwards, the HMI of each application will be designed. The third subsection relies on the explanation of the procedure for the image processing. Lastly, an analysis of the possible problems is preformed and respective solutions implemented.

6.1 Modification of Robot's Program

As exposed in Chapter 3, the 3D printing methodology at INEGI ends with the generation of a KRL code that is uploaded to the robot's controller. However, after each layer the robot is now supposed to position itself so that the camera captures a pertinent field of view and wait until it is intended. At this point, the KRL code was not prepared for these changes so it had to be modified. For this purpose, a function that runs on the robot controller every time a layer is finished was created. Figure 6.1 represents the grafcet of the function responsible for the camera positioning after each layer.

Each time a new layer was supposed to be deposited, the robot's function receives three arguments that are the coordinates for the camera position in x, y and z. In order to modify the KRL code and to calculate the appropriate values to pass to the function, a python script was developed. The python script opens the KRL code before it is uploaded to the robot's controller, and identifies whenever a new layer is going to be deposited by reading the layer height for each movement. Between each layer, the script adds a line that calls the function and passes the arguments. The x

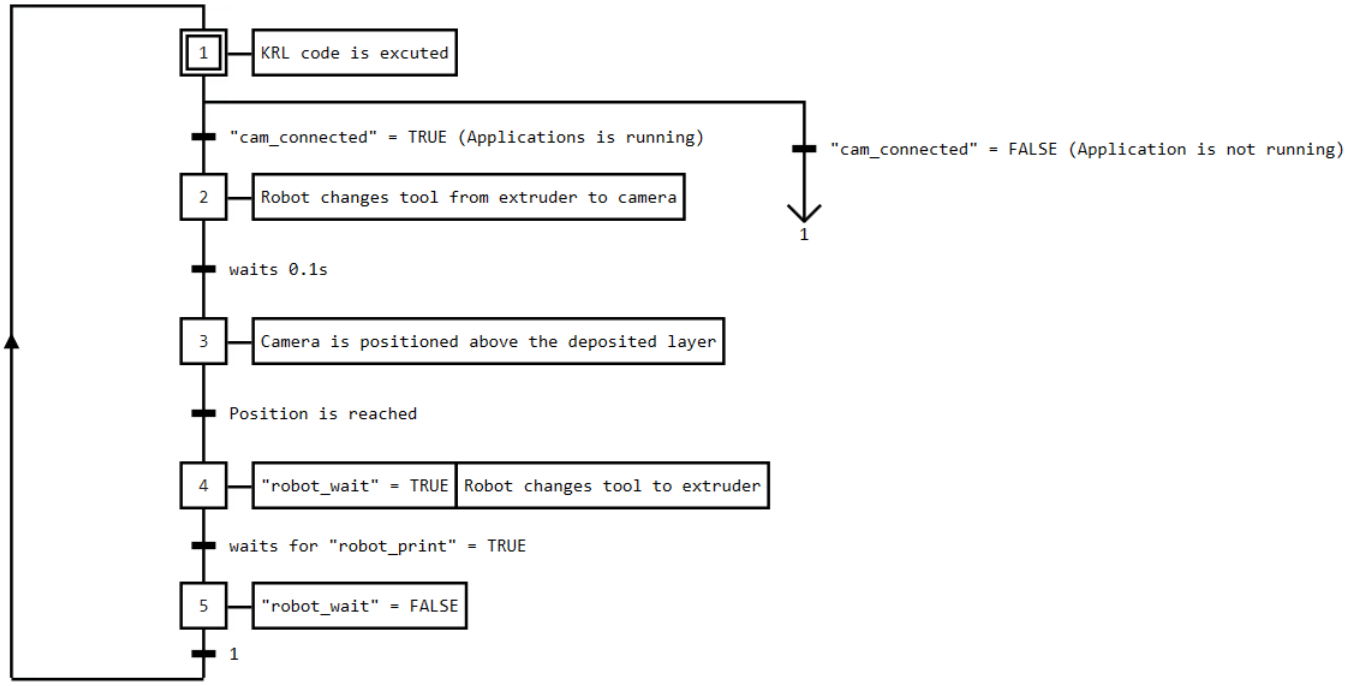

Figure 6.1: Grafcet of the robot function

and the y are the average values of each layer so that the object is centered on the image. Concerning the z value it is calculated by adding 10 mm more to the current layer height in order to get a focused image (as shown in Figure 6.2).

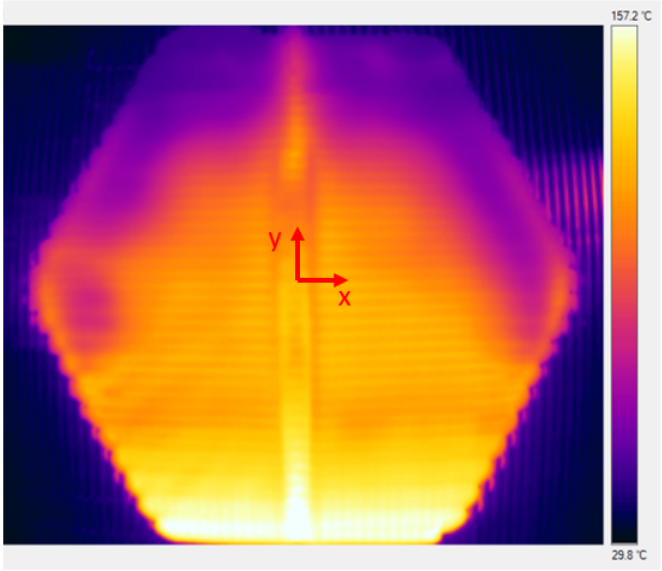

Figure 6.2: Example of a layer focused after it was deposited

In this example, the deposited layer is focused and well fitted in the image. This position, is accomplished by the following code segment on the KRL program:

```
...
# Coordinates of the layer's last points (Z=2)
LIN {X 94.300,Y 171.478,Z 2.000,A 90.000,B -0.000,C -180.000,S 6,T 50} C_DIS
LIN {X -94.300,Y 171.478,Z 2.000,A 90.000,B -0.000,C -180.000,S 6,T 27} C_DIS

# The extruder stops depositing material
TRIGGER WHEN DISTANCE=0 DELAY=0 DO extrude=FALSE

# The robot runs the function with the specified parameters
CAMERA_FUNCTION(0.000,0.000,2.000)

# Coordinates of the next layer's first points (Z=4)
LIN {X -93.808,Y -0.394,Z 5.000,A 90.000,B -0.000,C -180.000,S 6,T 27} C_DIS
LIN {X -93.808,Y -0.394,Z 4.000,A 90.000,B -0.000,C -180.000,S 6,T 27} C_DIS

# The extruder starts depositing material
TRIGGER WHEN DISTANCE=0 DELAY=0 DO extrude=TRUE

# Coordinates of the next layer's points (Z=4)
LIN {X -93.808,Y 0.432,Z 4.000,A 90.000,B -0.000,C -180.000,S 6,T 27} C_DIS
LIN {X -93.591,Y 6.469,Z 4.000,A 90.000,B -0.000,C -180.000,S 6,T 27} C_DIS
...
```

The camera function line was added to the program by the script. The values for X and Y are 0 since the object is centered in the origin of the coordinate system. The z value corresponds to a layer height of 2 mm plus 10 mm assuming that the camera is already 500 mm away accordingly to its calibration.

These modifications were crucial for the integration of the application in the system. This way, if one of the applications is running, the robot will follow this routine enabling waiting times between layers.

6.2 First Approach (Solution 1)

This section describes the line of thought and the development of the first application to execute the image processing and its interface with the user.

6.2.1 Relevant Considerations

The first step in the application development was to establish all the relevant factors that needed to be taken into account. In this case two main aspects were discussed: the camera and its data acquisition and the image processing method.

Considering the camera and its data acquisition, the ability to watch the image that the camera is getting is important to know in real-time what is the field of view that is being processed. Additionally, a color scale to represent the different temperatures detected was also considered to be crucial.

The camera measures the area contained in its FOV by assigning a value of temperature to each pixel of the image. So the output of the camera can be represented by a matrix on which each element, is a pixel. Naturally, not all pixels contain valuable information for this project, since only a defined region within the image is going to be studied. In this case, the region of interest are all pixels that contain information of the deposited layer. And, it was decided that those elements were going to be evaluated by the average of its values. It should be taken into consideration that the average temperature is probably the best analysis strategy since the geometry of the object printed can heavily influenced the cooling time. On Figure 6.3 it gets clear why it would not be viable to considerate the temperature of only a defined area of the deposited layer.

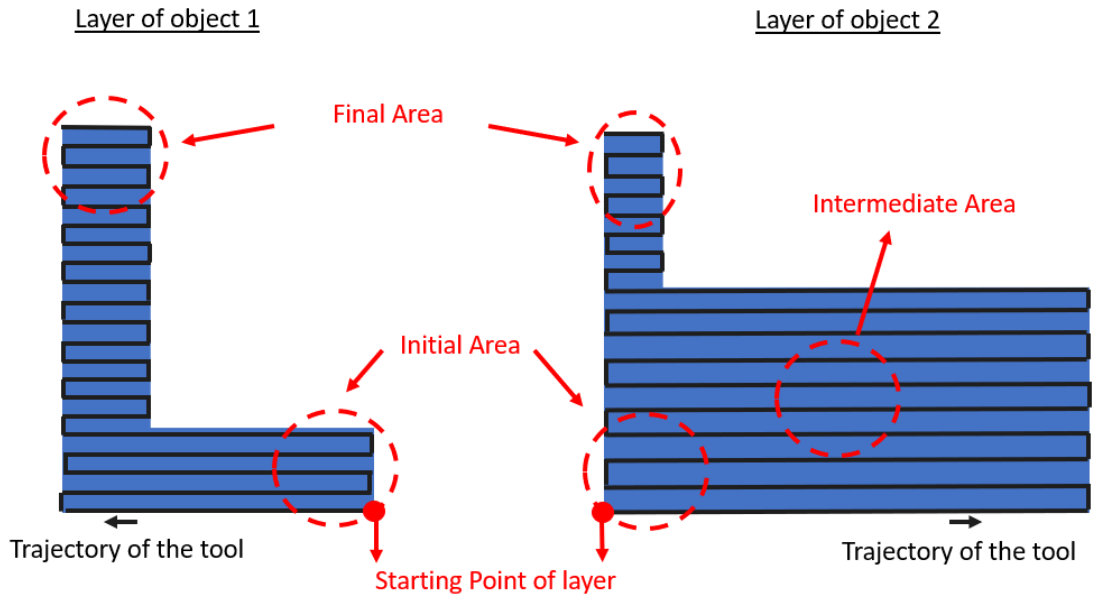

Figure 6.3: Example of geometry affected cooling times

Concerning the layer of the object 1 it can be considered that the cooling rate is approximately uniform due to its constant width. So, the final area and the initial area are going to take the same time to reach the same temperature. In this case, it would be viable to consider only one specific area like the initial one and, evaluate its temperature to compare to the chosen one. This would work because the final area would have reached the proper temperature by the time that the next layer is deposited on top of it. On the other hand, on the layer of object 2 the cooling rate on the initial, intermediate and final areas are completely different due to the quantity of material that is deposited on each region. So, let's imagine that only the temperature of the initial area is evaluated. When it reaches the chosen temperature, the printing continues but the intermediate area could be too hot and material would be deposited on top of it. If only the temperature of the intermediate area is considered, the time that is required so that it reaches the chosen temperature could be too much. Given this, the best compromise for all types of objects was to evaluate the average temperature of the whole deposited layer.

It was necessary to select a method for separating the significant information and the irrelevant one. There are a few steps concerning the image processing and a more detailed explanation is

done in Section 6.2.3. But, overall the following course of action was considered: When the application starts, it is required that an acceptable layer temperature is chosen by the user. Then, the KRL program starts and the robot deposits its first layer, and as shown previously, the robot runs its function, and positions the camera above the object that is being built. In that moment, the camera captures thermal images and data at a 60 Hz rate. When the first image is captured, the position of the pixels that are above the temperature selected by the user are stored. After that, every time an image is captured, the temperature of the pixels positioned on the stored coordinates are read. After each reading, an average of the temperature values is calculated. This means that every 0.1 seconds a new average temperature is computed and compared to the chosen layer temperature. When the average temperature of the pixels is equal or lower than the temperature chosen, the application communicates with *TwinCAT* and the KRL program continues. This is the method for image processing for each layer deposited.

After setting up which main aspects the application should include, it was important to reflect about how should the HMI be organized and what it should include.

6.2.2 HMI Design

A very important step of the solution development was to design an appropriate HMI so that the application is intuitive and simple to use. Figure 6.4 representes the HMI for the first approach.

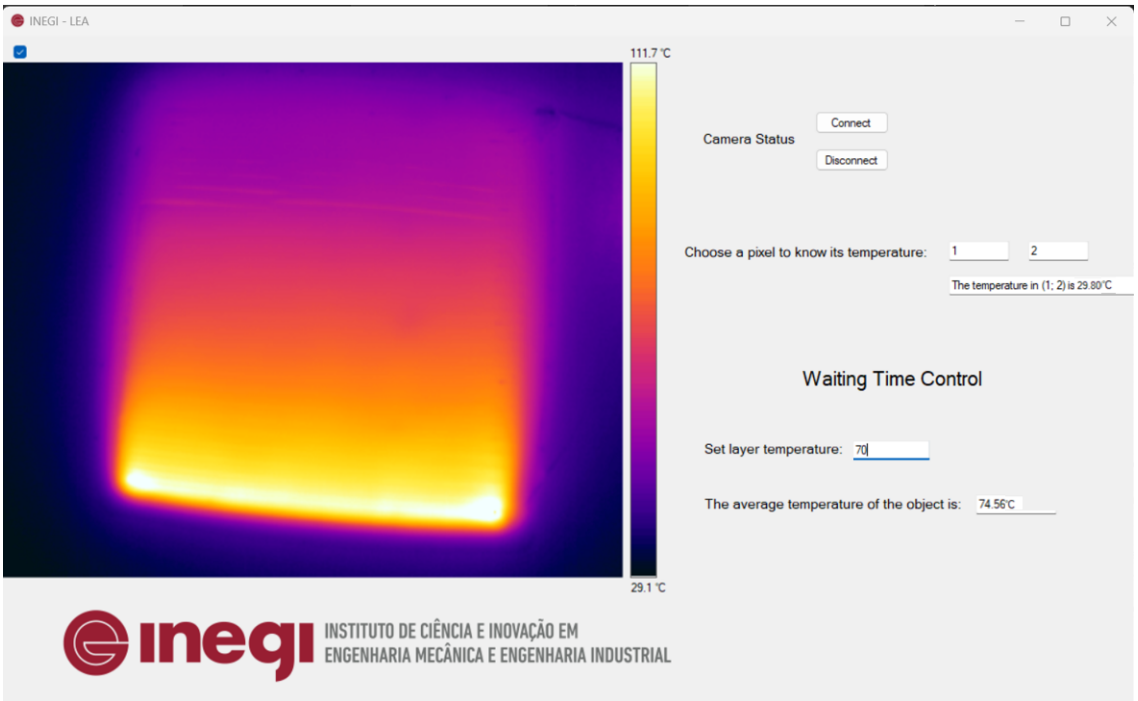

Figure 6.4: HMI of the first application developed

On the left, the live captured image is presented as well as its scale with minimum and maximum temperatures. On the right, there are some functionalities that were the base of the application. First, there are two buttons that change the status of the camera, it is possible to connect

either to the camera and observe the live captured image or disconnect from the camera and stop the image capturing. Bellow these two buttons there are two text boxes that access a pixel coordinate on the image matrix and a third text box retrieves the value of the temperature of the chosen pixel. This functionality was added in order to improve the knowledge of the C# programming language. Lastly, bellow the "Waiting Time Control" title are two text boxes labeled as: "Set layer temperature" and " The average temperature of the object is". The first one, will receive the value that the user defines as the ideal temperature for another layer to be deposited. The other one retrieves the current average temperature of the layer, determining whether the robot will proceed with the printing process or not.

6.2.3 Image Processing Algorithm

When the program starts, and the camera is connected through the button, it starts capturing data at 60 Hz. The image will be always visible on the HMI as previously established. Figure 6.5 represents a grafcet that demonstrates the image processing method on this approach.

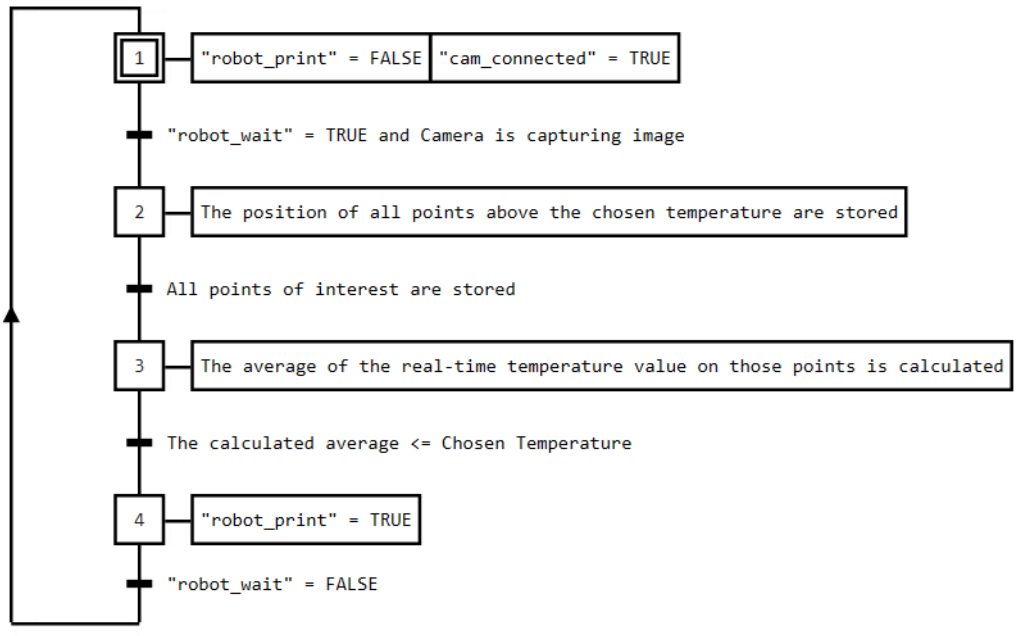

Figure 6.5: Grafcet of the image processing method on the first approach

When the application is executed the variables are set to the shown states and the user must write, on the appropriate text box, the ideal temperature that a layer should reach. Every 100 ms the state of the variable "robot_wait" is being checked and, when it changes to "true" the coordinates of all elements of the image matrix, with the value greater than the ideal chosen temperature, are stored on a list. Afterwards, every time that data is captured, the average of the temperature values on the list is calculated. This is repeated until the average value is equal or lower than the chosen temperature. When that happens, the state of the variable "robot_print" is set to "true" so that the

printing can continue. After the variable "robot_wait" is set to false, the program holds until the robot is waiting again.

6.2.4 Problems and Improvements

After testing the new system, some issues were considered as well as possible strategies to prevent their occurrence.

The first concern when analysing the system has to do with the criteria used to identify the elements of interest. When printing a large object, some areas can cool enough so it is already bellow the chosen temperature when the camera takes its first picture, which means that those points would not be taken into account on the average evaluation. This implies that there would also be an unnecessary increase of waiting time. To minimize this effect, instead of storing the points that are above the chosen temperature, all of the elements with a value higher than 30 °C were stored. Using to this strategy, not only the environment temperature points were eliminated but all the points of interest were considered.

Even though this approach can represent a good approximation of a solution for the problem, the image matrix elements that are considered can often be inaccurate. For instance, on Figure 6.6 some reflections are visible on the captured image. That area is above 30 °C, so it will be taken into account on the average calculation which is not accurate and can prolong the waiting time.

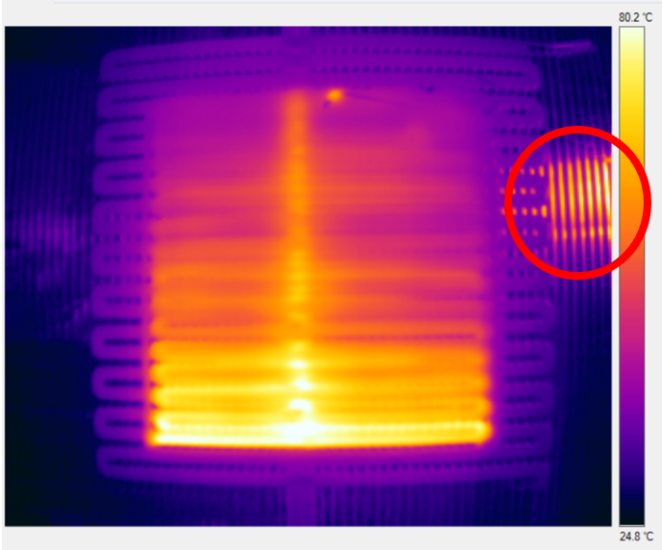

Figure 6.6: Reflection of the hot extruder on the table

For this reasons and because a more precise solution could be conceive, a second approach was developed.

6.3 Second Approach (Solution 2)

In this section it is explained how a new application was thought and implemented in order to create a more accurate solution.

6.3.1 Relevant Considerations

Developing this second application, all of the considerations taken into account on the first one were also implemented. The camera's point of view is always observable on the HMI and the average temperature method was also maintained. Some other aspects were added so that the pixels that are analyzed belong, in fact, to the object that is being built. Additionally, with the first application all of the deposited layer was used on the calculations, not having in consideration that the next layer can be very different. This means that the robot would wait more than it should if the area that is going to be printed on top of is already cooled enough. So, a look ahead method was also introduced.

To achieve these goals, a pre-processing data algorithm was created. On the HMI of the application, the KRL code can be uploaded and it is sequentially divided layer by layer. Every point that the robot is going to extrude on the printing table, is stored and converted to the image pixel space. So when the robot is waiting and the camera is acquiring data, the pixels considered to the processing are only the ones that belong to the area of the next layer. This allows the system to wait just the necessary time, until the area where the next layer is going to be printed reaches the chosen temperature.

Lastly, the option to save an external file with data about the process control was added, to allow the user to see how the process evolved over time. On this file it is possible to consult how long was the waiting time and how the average temperature evolved, for each layer.

6.3.2 HMI Design

The HMI for this application presents some modifications as shown on Figure 6.7.

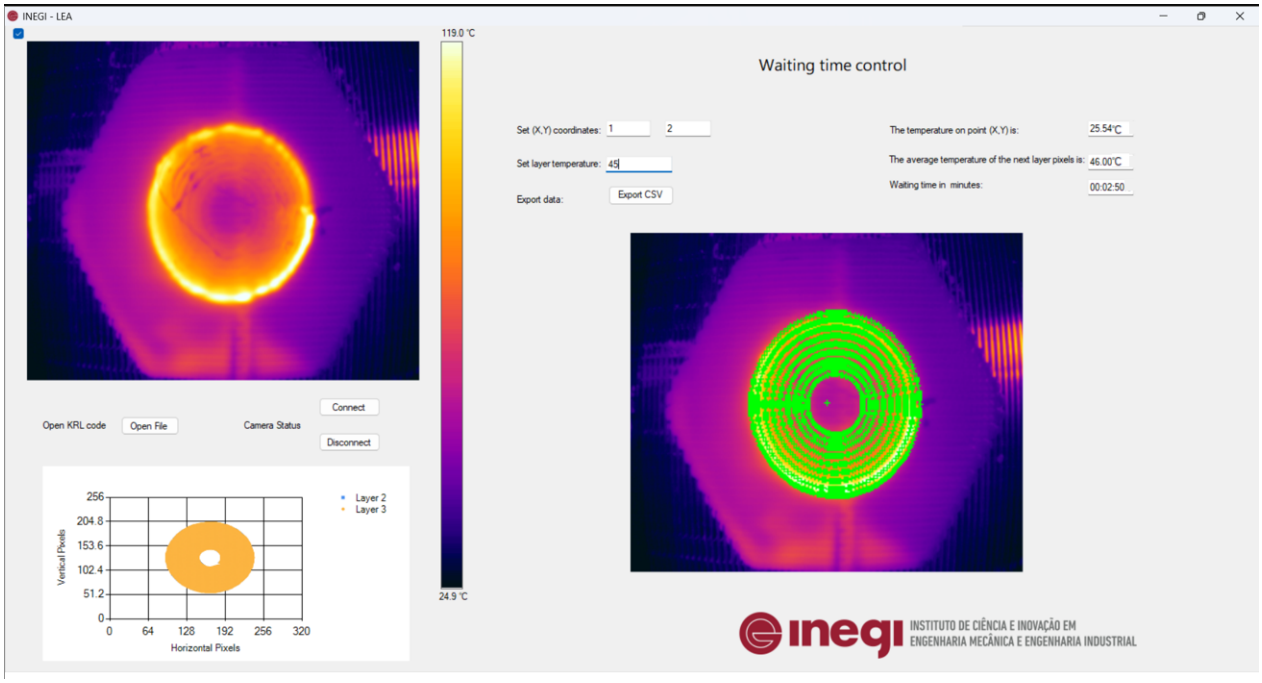

Figure 6.7: HMI of the second application developed

Bellow the live image of the camera, there is a coordinate system. Its axes represent the image length and width so it is clearer where the points of interest were positioned on the image. In between are the same "Connect" and "Disconnect" buttons to turn on and off the live image and also, a new button "Open file". This new interface element is used to upload the KRL code so that the pre-processing is possible. To make sure the user uploads the file before connecting the camera, the button "Connect" is disabled until the pre-processing is done.

On the right, three new elements were included: an "Export CSV" button, a text box that shows how much time is the system waiting and another live image in which the user can see which area of the layer is being analyzed. The points refresh accordingly to the layer that the system is working on. The coordinate system was the first indicator of the area of interest, however there was a necessity of adding the live image with the layer indicator so that the points of interest were clearer.

All of the other elements are the same as previously explained.

6.3.3 Image Processing Algorithm

In this case, the image processing algorithm depends on the data pre-processing so it is relevant to explore that step.

When the button "Open file" is pressed and the KRL code is uploaded, all lines written are read and all points where the extrusion happens are stored. Figure 6.8 shows the method that was implemented to store all points of interest.

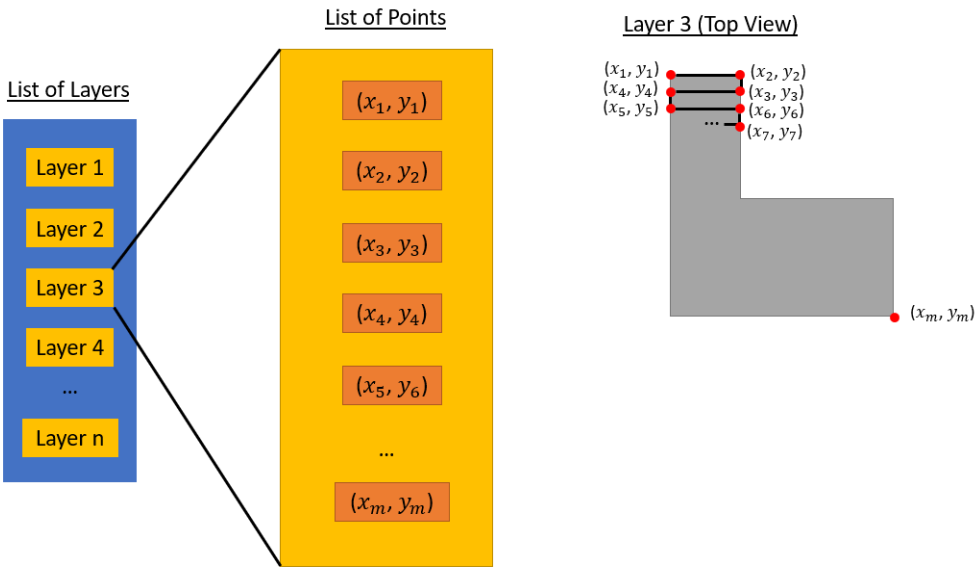

Figure 6.8: Method for storing points of interest

After the file is read, a list of points for each layer is created and stored on another list. In only one list it is possible to access every layer of the object to be printed and the coordinates of each point that the extruder is going to travel to. Also, a list of the height for each layer is also generated.

The points stored are on the coordinate system of the robot, so the next step was to convert those points into image pixels. On Figure 6.9 the top and front view of the image capturing system is represented. The red elements correspond to the camera and image space while the black ones are associated with the printing table and robot coordinate system.

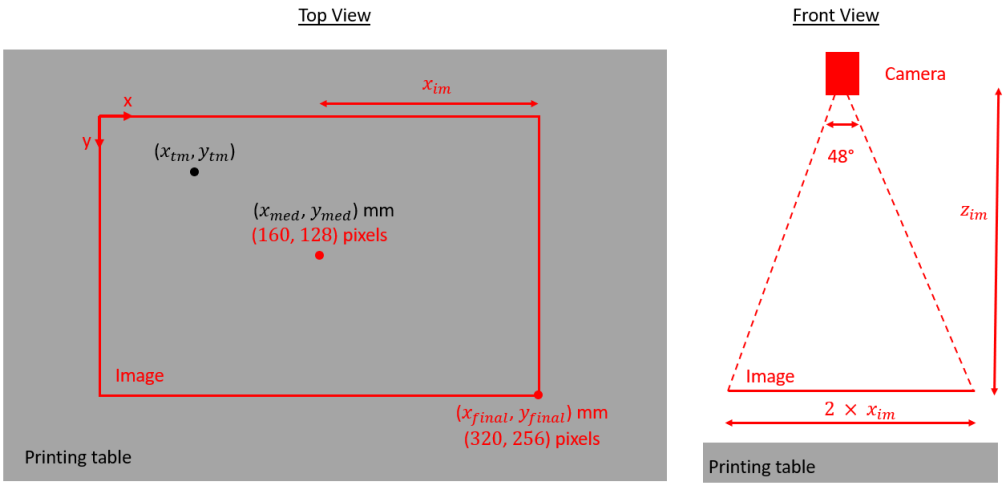

Figure 6.9: Top and front view of the image capturing system

On the printing table, there is a point that belongs to the object being printed with the coordinates (x_{tm}, y_{tm}) and the camera is centered on the coordinates (x_{med}, y_{med}) which is the center of the layer. The height of the camera is always adjusted so that all points of interest are captured on the image. The dimensions of the image in mm can be calculated knowing the distance between the camera and the points of interest. The width and height of the image in mm can be obtained by multiplying the height of the camera z_{im} and the tangent of the angle of view in each direction. For instance, considering the x axis, using the tangent of 48° the width of the image ($2x_{im}$) in mm can be calculated. The same process for the y axis is valid with the angle of view of 39°. Both the dimension of the image in mm and pixels are known and the center of the image always coincides with the average coordinates (position of the camera according to the function arguments) on the robot space. A relation between the image space and the printing table space on x and y axes can be defined by the equations:

$$x_{ip} = \frac{x_{tm} - (x_{med} - x_{im})}{2x_{im}/320} \tag{6.1}$$

$$y_{ip} = \frac{y_{tm} - (y_{med} - y_{im})}{2x_{im}/256} \tag{6.2}$$

x_{ip} and y_{ip} being the coordinates of the point on the image in pixels (according to the coordinate system represented).

This method was applied to each point so that it is known where all the points will be located on the image.

While executing the KRL program, the robot travels between the instructed point. This implies that not only its positions have to be converted to the image space, but also the coordinates of the points forming the connecting lines (shown on figure 6.10).

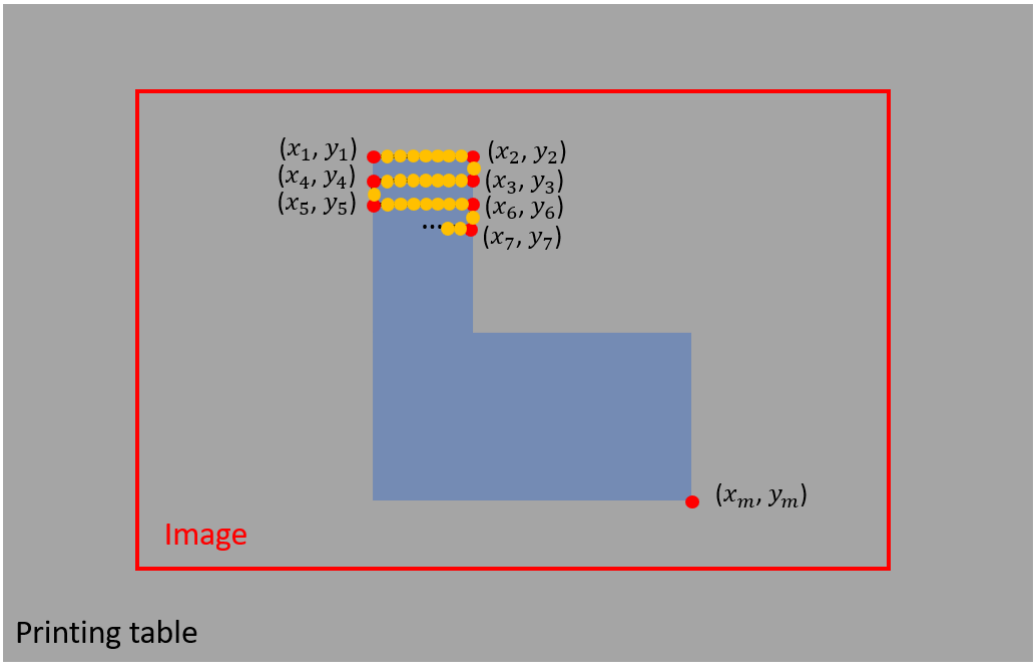

Figure 6.10: Representation of the points of interest on the image

The red marks were the points initially stored on the lists, however, the yellow points are part of the layer as well, simply do not appear on the KRL code for storage because the robot travels with linear moves from a point to another. Having the red points already converted to pixels on the image space, it is necessary to store also the yellow points so that the whole layer can be analyzed. For each layer and pixel position stored, the following instructions were defined: If either the x or y coordinates were the same as the next pixel on the list, all of the pixel coordinates that belong to the line that connects them is stored on the list of the pixels of interest. If both of the x and y coordinates were different, the slope of the line is calculated and all of the pixel that belong to it are also stored. After this step, all of the pre-processing is completed and the camera can be connected so that the image analysis can occur when it is supposed to.

On Figure 6.11 the grafcet of the image processing method is represented.

On this algorithm a layer counter was implemented and initialized at 2 since the pixels that are going to be analyzed are the ones that belongs to the next layer. So, when "robot_wait" changes its state to "true", the pixels stored on the list for the corresponding layer number are accessed. And only those pixel's values are considered on the average calculation. When the average value reaches the chosen temperature, the variable "robot_print" is set to "true" and the layer counter increases its value by 1. This is repeated until the object is fully built.

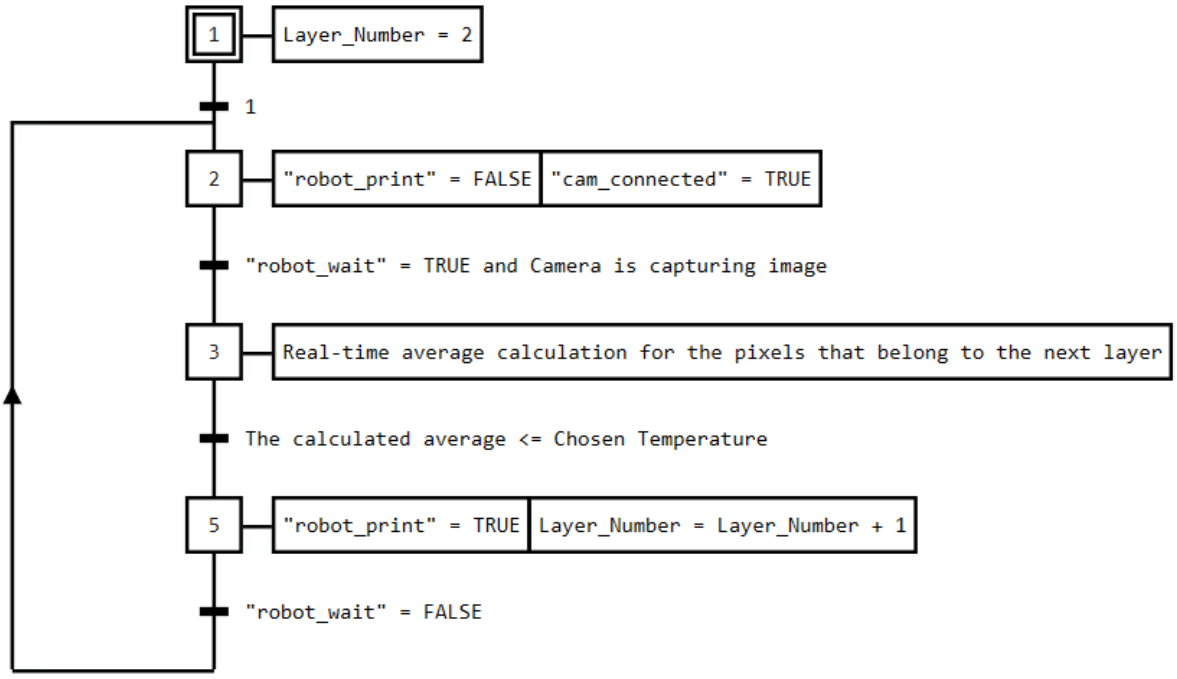

Figure 6.11: Grafcet of the image processing method on the second approach

6.3.4 Problems and Improvements

Even though this approach is much more accurate than the first one, there was one main aspect that was necessary to improve. If, for some reason, the application crashed, there was no way of restarting at the same point as it stopped. To solve this problem, a new text box was added to the HMI. The goal of the text box is to keep track of the layer number during the process and, in case of failure it was also possible to write on the text box the number of the layer were it last stopped so that the process can continue at the same point it was left. Also, the graph that was part of the HMI was taken out, since the live image with the representation of the pixels analyzed and the text box with the layer number give the same information in a clearer way (Figure 6.12).

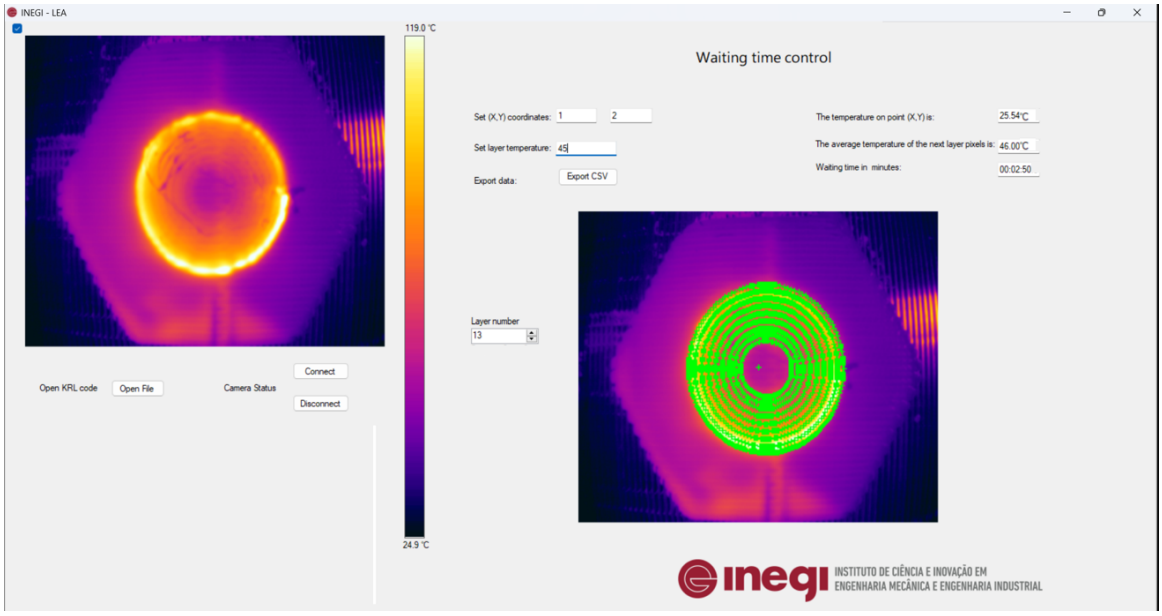

Figure 6.12: Improved HMI for the second approach

Chapter 7

Experiments

The goal of this section is to show the tests perfomed to the solution developed and demonstrate the impact it can have on a 3D printing process. To begin the experiments, an object was defined and printed without any temperature control applied. Then, the same object was manufactured applying the solution developed. Lastly, an evaluation and comparison of the results was executed.

7.1 Definition of the Object and Process Parametrization

Figure 7.1 presents the object that was tested and on Appendix E can be found the definition drawing.

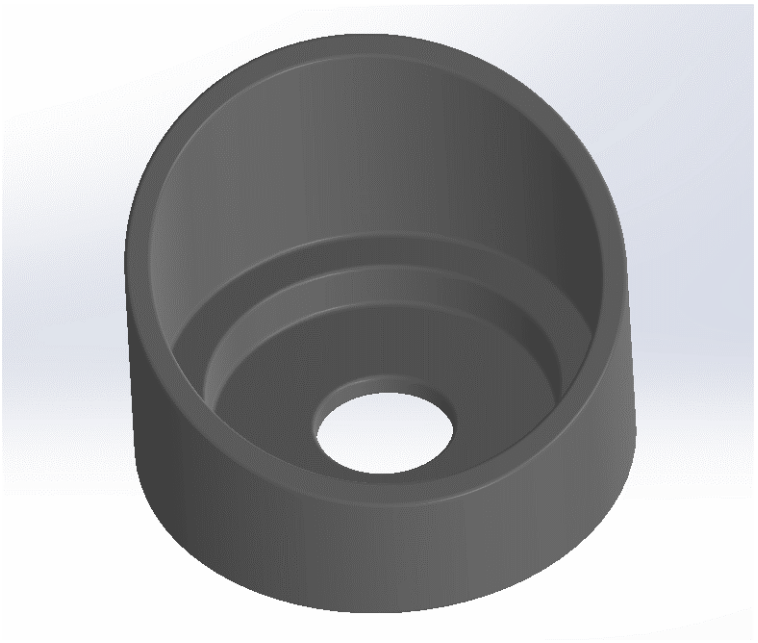

Figure 7.1: Object to be printed on the tests

The object is simple but it still presents different sections. On the bottom, the geometry is more compact meaning that more material is deposited in the beginning. And, as going up on

the object, the sections become thinner so the layers deposited should be smaller. This type of features allowed the system to show its behavior on different scenarios. The top geometry is really interesting since it is composed by a relatively thin wall, that means that a minor printing time is necessary, so a higher waiting time is expected. While building this feature, the temperature control should play a crucial role since the part can fail due to lack of rigidity.

The object was sliced in 65 layers of material. Concerning the process parameters, a 5 mm nozzle was used, a 2 mm layer height was defined and the robot velocity was 40 mm/s. The printing material was a Polyhydroxyalkanoate (PHA) and it was extruded at 190°C. It is biodegradable and it has the potential to substitute conventional plastics.

7.2 Printing Without Temperature Control

In a first instance, the object was printed without any temperature control. The temperature of the room was 19°C and the printing took 1 hour and 32 minutes. Figure 7.2 shows the object printed on the described conditions.

Figure 7.2: Printing without temperature control

As the figure demonstrates, the first layers of the object are rigid enough to take the weight of the following ones so no temperature defects were detected. The base of the object is visibly bowed due to an unexpected lack of adhesion of the material to the table. The last layers of the object started to deform due to the weight of the top layers. As expected, without the temperature control, the object was not successfully printed.

7.3 Printing with Temperature Control

To preform the experiment with the temperature control it was necessary to setup the computer on the lab where the robot was and connect the Ethernet cable to it. Before the robot starts running the modified KRL code on its controller, the application was executed and the same KRL file was uploaded to it in order to get the pre-processing done. Afterwards, the camera was connected and the robot started to run its program. The chosen temperature for the layers was initially 60°C, although later it was necessary to adjust it to 75°C since delamination defects started to appear. The temperature of the room was 20°C and the printing took 3 hours and 17 minutes. After the object was built it was possible to get access to the csv file where the evolution of the average temperature for each layer and the waiting time were registered. On Figure 7.3 the finished printed object is shown.

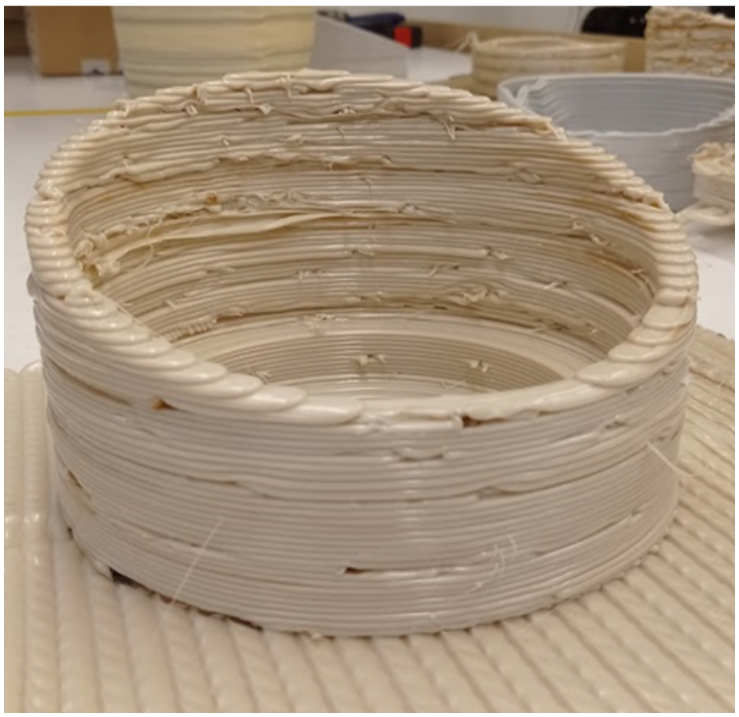

Figure 7.3: Printing with temperature control

As the figure illustrates, the object presents some defects due to the PHA fluidity. Some delamination defects are observable on the first layers because the temperature chosen was too low, so on the next layers this temperature was increased. However, all layers were deposited on top of rigid material which resulted in a successful printing.

During the printing, it was possible to capture some images (figure 7.4) of different layer analysis in order to better understand which type of section was being evaluated.

The different sections during the printing varied the following way accordingly to the image: from 2 to 6 a more compact geometry is printed, from 7 to 16 the thickness of the object decreased, from 17 to 31 only a wall of 10mm was deposited and finally, from 32 to 65 the same wall opened until the final geometry was reached.

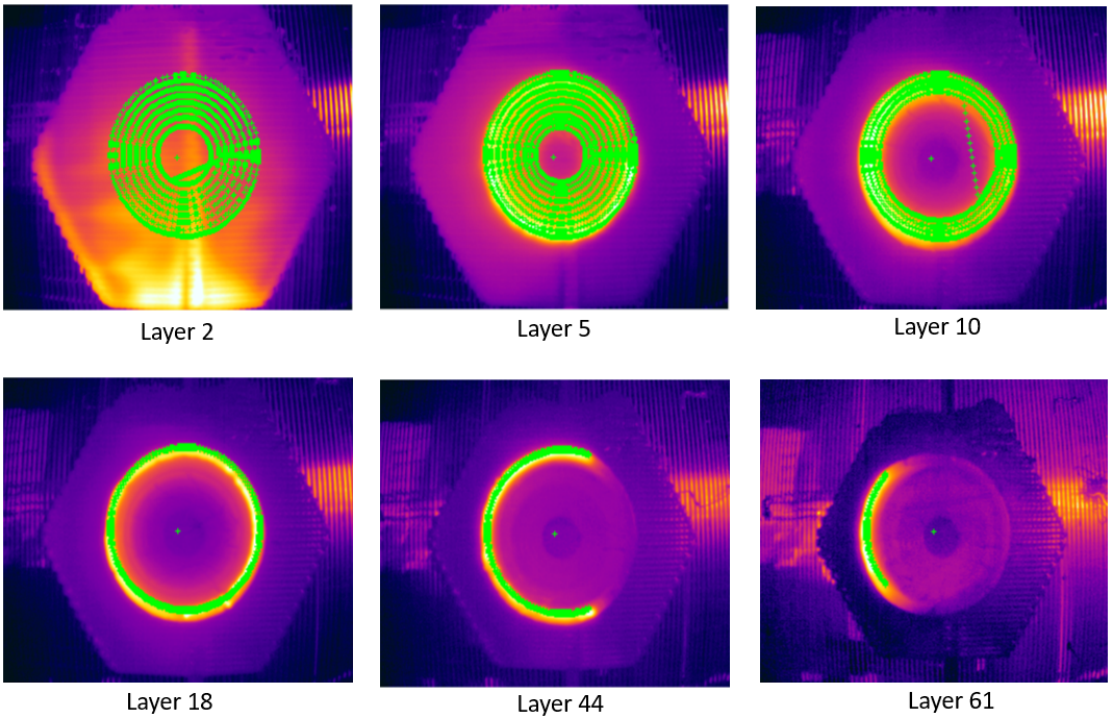

Figure 7.4: Printing with temperature control

After the process, it was possible to trace the graph of Figure 7.5, that illustrates the waiting time for each layer during the deposition.

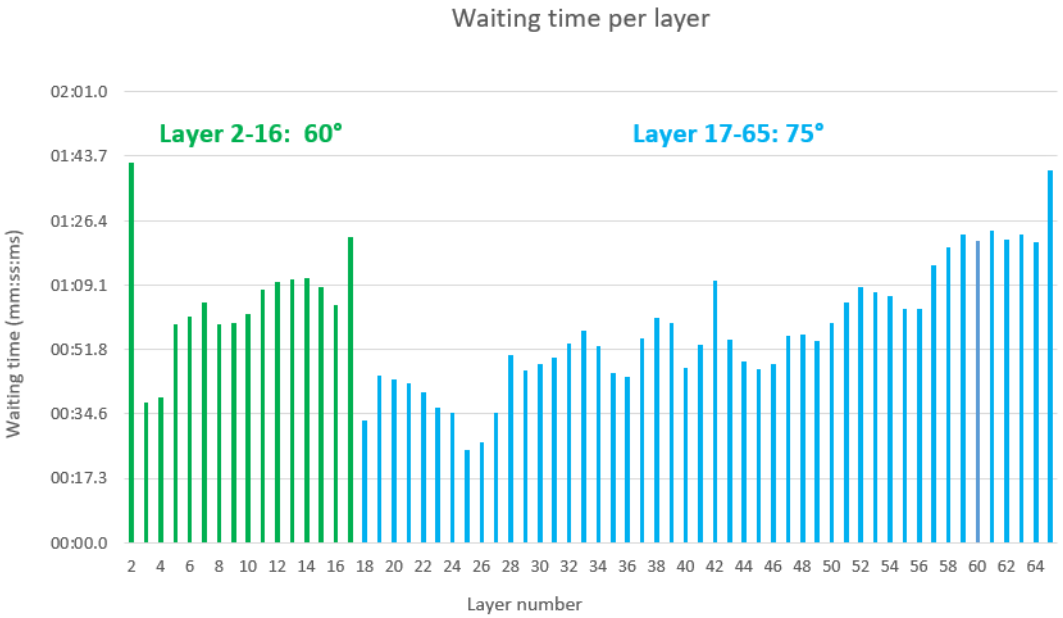

Figure 7.5: Different stages of the printing process

From layer 1 to 16 the temperature that the layer should reach was 60°C. After observing some delamination, it was concluded that this value was too low for material to bond. For the subsequent

layers, this temperature was increased to 75°C which seemed to fix the problem. After the first layer was deposited, the waiting time was about 1 minute and 42 seconds which was the longest wait that was registered. The deposited layer was not part of the object itself; instead, it served as a compact base on which the object was printed, as shown on Figure 7.4. The part was printed on the center of the base so it took longer to cool down since the application evaluates only the area where the next layer is going to be deposited. Until layer 17 the waiting times were longer since the temperature that the layers should reach was lower. However, maybe longer waiting times could be justified since more material is deposited and the heat release could be slower leading to a longer time to reach a certain value. Overall, the tendency of the waiting time was to increase since the layer area was getting smaller and the next layer was on top of the one that got deposited before. If the layer is smaller, there is barely any time for it to cool down before the robot finishes the layer, which increases the waiting time. The average waiting time per layer, in this process, was 58 seconds.

Concerning the evolution of the average temperature of the layers, on Appendix F a graph is presented. As commented before, it is visible that after the 16th layer, the temperature was increased from 60°C to 75°C. It is also noticeable that as the layers were becoming smaller, the initial temperature was increasing since there was not sufficient time for the material to cool down during printing. Additionally, it is noticeable that layers that look alike tend to have nearly the same initial temperature, meaning that the cooling rate is very similar.

7.4 Results Discussion

When comparing the object manufactured without and with temperature control the difference is clear, as illustrated on figure 7.6.

By looking to the object a), the failure of printing the thinner wall is evident. The hot material deposited on top of layers that were not rigid enough, resulted in material to fall down. The object b), was built by a temperature controlled printing. With the modifications on the robot and the application, the part was printed with success. Even though the a) process was almost half of the time on the same environment conditions, it was not possible to achieve a good quality part. The weight of the last layers could not be supported by the previously deposited material which lead it to collapse. However the b) process took twice as long to finish, a quality object was built, demonstrating that the waiting time implementation solved the issue that prompted this dissertation.

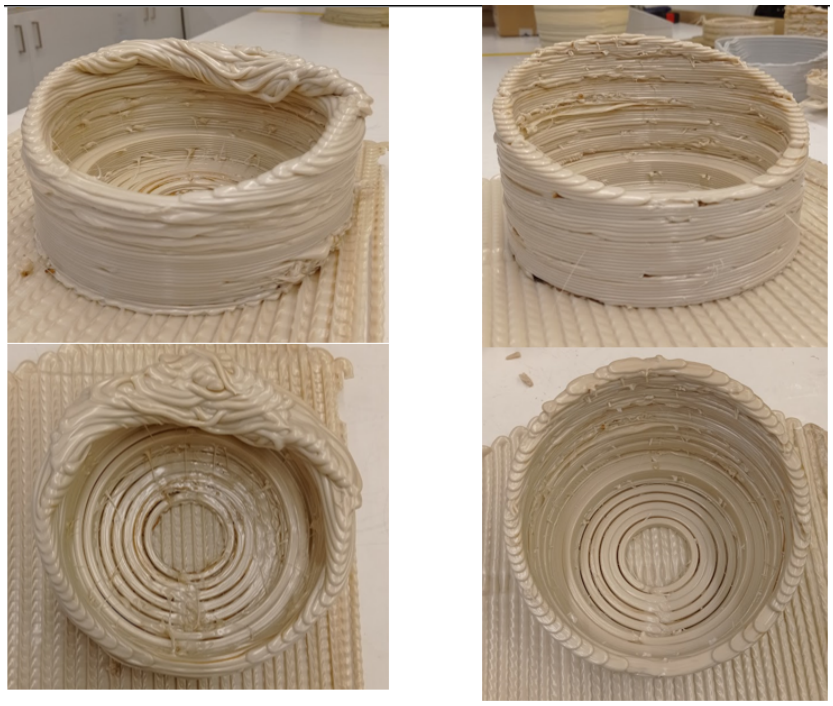

Figure 7.6: Object printed: a) without temperature control b) with temperature control

Chapter 8

Conclusions and Future Works

8.1 Conclusions of the Project

The conducted project demonstrated a successful approach to temperature optimization during deposition using a thermal camera.

Initially, this dissertation was divided into three main objectives, these being: the design of a camera support, development of an application to control the camera's measurment process and the modification of the robot routines accordingly to the data acquired by the camera. All of the goals were accomplished during different states of the project execution. Concerning the application development, it was a challenge to program the image and KRL code processing algorithms since a lot of tests were needed to ensure that the data manipulation was done correctly. Finally, considering the robot routine modifications, since lines with arguments to the function were added after each layer, before deployment, it would be confirmed that everything was valid. It is possible to conclude that the objectives proposed for the dissertation were achieved.

Considering the project's implementation, it presents some advantages as well as disadvantages. While adding waiting times during the process may increase printing time, it ensures the production of high-quality objects and reduces the risk of mid-manufacturing failures, minimizing material waste. Unlike the traditional printers, the system used for this project is not capable of preforming material retraction. So, while the camera is acquiring data, the extruder would release small amounts of material that remain inside of the tool. However, the quantity of material dispensed by the extruder while the robot is waiting is much less than the material that would go to waste if a print failed halfway through the process. These findings and observations are consistent with Borish *et al.* [19] except for the overall printing time that was, in this project, significantly smaller since the material used was different.

The project developed using the IR camera was a successful approach for solving the problem. When the process ends, the data can even be stored and analyzed. Additionally, because the HMI allows the user to chose any layer temperature, this application can be used for every material.

8.2 Future Works

For future works, it would be interesting to add active cooling in order to minimize the waiting time. Adding external fans as mentioned previously gets into conflicts with the extruder controller. The incorporated cooling system of the tool did not fix the problem since the air that is supposed to cool off the material passes through the heating zones of the extruder, transferring heat to the air. So, to fix this issue, the source of air had to be external to the system, ensuring that it is cold enough to provide a significant cooling rate to the deposited material. Additionally, it should be pointed to the opposite direction of the nozzle to not interfere with the heating control. Another possible solution is to replace the average temperature analysis of the pixels for a system that would attribute different weights to the distinct areas based on a thermal model. So, it would be possible to predict when the layer is sufficiently cooled down. This way, no excessive waiting times are implied. Additionally, some system that could test the chosen layer temperature before starting the process would be really useful. To be able to test different layer temperatures and its influence on the quality of the object printed can minimize defects.

References

[1] Julien Gardan. Additive manufacturing technologies: state of the art and trends. pages 149–168. CRC Press, 2017.

[2] Ian Gibson, David Rosen, and Brent Stucker. *Additive manufacturing technologies*. Springer New York, 2014.

[3] Eric Barnett and Clément Gosselin. Large-scale 3d printing with a cable-suspended robot. *Additive Manufacturing*, 7:27–44, 2015.

[4] Tian-Ming Wang, Jun-Tong Xi, and Ye Jin. A model research for prototype warp deformation in the fdm process. *International Journal of Advanced Manufacturing Technology*, 33:1087––1096, 2007.

[5] Mohammadreza Lalegani Dezaki, Mohd Khairol Anuar Mohd Ariffin, and Saghi Hatami. An overview of fused deposition modelling (fdm): Research, development and process optimisation. *Rapid Prototyping Journal*, 27(3):562–582, 2021.

[6] Brett G Compton, Brian K Post, Chad E Duty, Lonnie Love, and Vlastimil Kunc. Thermal analysis of additive manufacturing of large-scale thermoplastic polymer composites. *Additive Manufacturing*, 17:77–86, 2017.

[7] Xin Wang, Man Jiang, Zuowan Zhou, Jihua Gou, and David Hui. 3d printing of polymer matrix composites: A review and prospective. *Composites Part B: Engineering*, 110:442–458, 2017.

[8] Yanzhou Fu, Austin Downey, Lang Yuan, Avery Pratt, and Yunusa Balogun. In situ monitoring for fused filament fabrication process: A review. *Additive Manufacturing*, 38:101749, 2021.

[9] Hamid Reza Vanaei, Mohammadali Shirinbayan, Michael Deligant, Sofiane Khelladi, and Abbas Tcharkhtchi. In-process monitoring of temperature evolution during fused filament fabrication: A journey from numerical to experimental approaches. *Thermo*, 1(3):332–360, 2021.

[10] Charoula Kousiatza and Dimitris Karalekas. In-situ monitoring of strain and temperature distributions during fused deposition modeling process. *Materials & Design*, 97:400–406, 2016.

[11] Jun Yin, Chaohua Lu, Jianzhong Fu, Yong Huang, and Yixiong Zheng. Interfacial bonding during multi-material fused deposition modeling (fdm) process due to inter-molecular diffusion. *Materials & Design*, 150:104–112, 2018.

[12] Hamid Reza Vanaei, Mohammadali Shirinbayan, Sidonie Fernandes Costa, Fernando Moura Duarte, José António Covas, Michael Deligant, Sofiane Khelladi, and Abbas Tcharkhtchi. Experimental study of pla thermal behavior during fused filament fabrication. *Journal of Applied Polymer Science*, 138(4):49747, 2021.

[13] David Xu, Yancheng Zhang, and Franck Pigeonneau. Thermal analysis of the fused filament fabrication printing process: Experimental and numerical investigations. *International Journal of Material Forming*, 14:763–776, 2021.

[14] Fabio Caltanissetta, Gregory Dreifus, Anastasios John Hart, and Bianca Maria Colosimo. In-situ monitoring of material extrusion processes via thermal videoimaging with application to big area additive manufacturing (baam). *Additive Manufacturing*, 58:102995, 2022.

[15] Jonathan E Seppala and Kalman D Migler. Infrared thermography of welding zones produced by polymer extrusion additive manufacturing. *Additive manufacturing*, 12:71–76, 2016.

[16] Eleonora Ferraris, Jie Zhang, and Brecht Van Hooreweder. Thermography based in-process monitoring of fused filament fabrication of polymeric parts. *CIRP Annals*, 68(1):213–216, 2019.

[17] Arthur Lepoivre, Nicolas Boyard, Arthur Levy, and Vincent Sobotka. Heat transfer and adhesion study for the fff additive manufacturing process. *Procedia Manufacturing*, 47:948–955, 01 2020.

[18] Ralph B. Dinwiddie, Vlastimil Kunc, John M. Lindal, Brian Post, Rachel J. Smith, Lonnie Love, and Chad E. Duty. Infrared imaging of the polymer 3D-printing process. In Fred P. Colbert and Sheng-Jen Tony Hsieh, editors, *Thermosense: Thermal Infrared Applications XXXVI*, volume 9105 of *Society of Photo-Optical Instrumentation Engineers (SPIE) Conference Series*, May 2014.

[19] Michael Borish, Brian K. Post, Alex Roschli, Phillip C. Chesser, Lonnie J. Love, Katherine T. Gaul, Matthew Sallas, and Nikolaos Tsiamis. In-situ thermal imaging for single layer build time alteration in large-scale polymer additive manufacturing. *Procedia Manufacturing*, 34:482–488, 2019. 47th SME North American Manufacturing Research Conference, NAMRC 47, Pennsylvania, USA.

[20] General tips - RoboDK Documentation. https://robodk.com/doc/en/General.html. (accessed: Mar. 29, 2023).

[21] Mondi Anderson. What is EtherCAT (Ethernet for Control Automation)? https://realpars.com/ethercat/, Mar 2019. (accessed: Apr. 4, 2023).

[22] EtherCAT Technology Group. EtherCAT Automation Protocol Stack. https://www.ethercat.org/en/products/30083F1CDAFA4E269B3C57E64A4C2D18.htm. (accessed: Apr. 4, 2023).

[23] Beckhoff Information System - ADS Communication. https://infosys.beckhoff.com/english.php?content=../content/1033/cx8190_hw/5091854987.html. (accessed Apr. 11, 2023).

[24] Beckhoff Information System - Access Data via Symbolic path. https://infosys.beckhoff.com/index.php?content=../content/1031/tcadsnetref/7312577675.html&id=. (accessed Apr. 11, 2023).

Appendix A

KUKA Robot Datasheet

KR 50 R2100

Technical data

Maximum reach	2101 mm
Rated payload	50 kg
Maximum payload	61 kg
Maximum supplementary load, rotating column / link arm / arm	50 kg / 30 kg / 30 kg
Pose repeatability (ISO 9283)	± 0.05 mm
Number of axes	6
Mounting position	Floor; Ceiling; Wall; Desired angle
Footprint	603 mm x 480 mm
Weight	approx. 533 kg

Axis data

Motion range	
A1	±185 °
A2	-175 ° / 60 °
A3	-120 ° / 165 °
A4	±180 °
A5	±125 °
A6	±350 °
Speed with rated payload	
A1	180 °/s
A2	175 °/s
A3	175 °/s
A4	250 °/s
A5	250 °/s
A6	360 °/s

Operating conditions

Ambient temperature during operation	0 °C to 55 °C (273 K to 328 K)

Protection rating

Protection rating (IEC 60529)	IP65
Schutzart Arm (IEC 60529)	IP65 / IP67
Protection rating, robot wrist (IEC 60529)	IP65 / IP67

Controller

Controller	KR C5; KR C4

Certificates

ESD requirements	IEC61340-5-1; ANSI/ESD S20.20

Workspace graphic

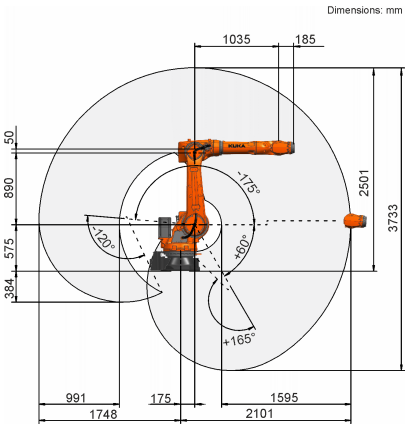

Payload diagram

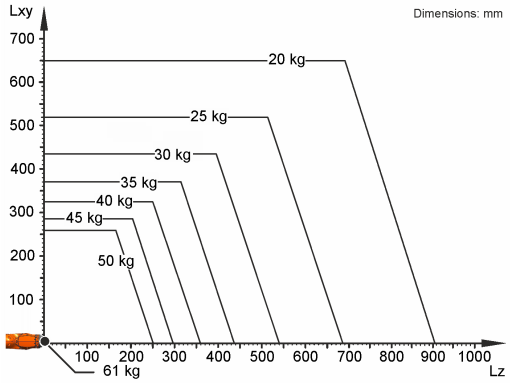

The KR 50 R2100 is designed for a rated payload of 50 kg in order to optimize the dynamic performance of the robot. With reduced load center distances and favorable supplementary loads, a maximum payload of up to 61 kg can be mounted. The specific KUKA Load case must be verified using KUKA. For further consultation, please contact KUKA Service.

Mounting flange

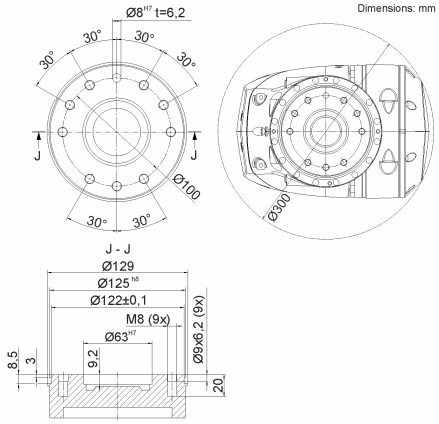

0000-332-115 / V6.1 / 19.01.2023 / en
KUKA Deutschland GmbH Zugspitzstrasse 140, 86165 Augsburg, Germany. Tel.: +49 821 797-4000, www.kuka.com

Appendix B

CEAD Extruder Datasheet

TECHNICAL DETAILS

E25 robot extruder		**Upgrades**
Dimensions (mm)	230x340x980	
Weight (kg)	30	
Screw diameter (mm)	25	
Material transport (m)	10	20
Heat zones	4	
Cooling zones	1	
Heating power (kW)	2.45	
Temperature (°C)	310	400
Drive system	Siemens servo	
Power servo (kW)	0.75	1
Max output (kg/h)	12 *	
Nozzle size (mm)	2-18	
Layer width (mm)	3-30	
Layer height (mm)	1-9	

Control cabinet		
Communication	Analog-digital	Profinet
Operator control	Siemens Simatic HMI	
Material storage (L)	± 60	
Software	CEAD custom	

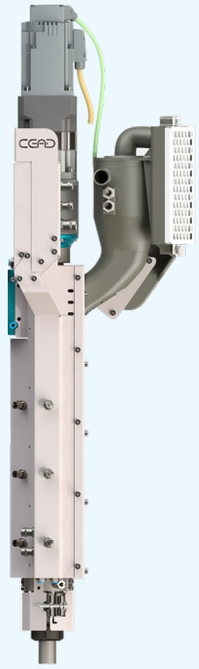

CEAD Software
The CEAD software is directed to material processing and controls, including material transport, heat zone PID control, water cooling and overall safe operations of the extruder.

HMI
Allows extruder control, quick selection and saving of pre-set material recipes, tracking of temperature -, speed -, alarm - and torque logs, system diagnostics and monitoring operating statistics.

* Measured with PP 30% glass fiber

ANCILLARY SYSTEMS

To maximize your workflow and completely furnish your robotic cell, we offer additional technology components.

Pellet dryer
The pellet dryer is required when processing various thermoplastic materials. *Optional: automated hopper loader for easy material loading and continuous 24/7 operations.*

Print bed
The proprietary print bed facilitates a non-permanent mechanical bonding feature between the printed part and print surface. The CEAD solution provides a rigid and easy-to-use build platform.
Optional: multiple sizes and/or heated bed upgrade available.

Extruder mount
Easy to install parking spot for the extruder when the robot is used for multiple processes.

MATERIALS

CEAD offers a wide variety of fiber reinforced plastic materials for different kind of applications. Find our latest materials brochure and up to date material offerings. All materials are supplied in pellets.

Biobased materials
Materials such as PLA/PP combined with cellulose fibers.

Commodity materials
The usual suspects PP/ABS/ASA/PET/PC combined with glass fibers.

High-end materials
For ultra strong parts PEEK/PESU/PPS combined with carbon fiber.

Appendix C

Thermal Camera Flir A35 Datasheet

SPECIFICATIONS

Image and Optical Data	A35	A65
IR Resolution	320 x 256	640 x 512
Thermal Sensitivity/NETD	<0.05°C @ 30°C (86°F) / 50 mK	
Image Frequency	60 Hz	30 Hz
Focus	Fixed	
Detector Data		
Detector Type	Uncooled VOx microbolometer	
Spectral Range	7.5 – 13 µm	
Detector Pitch	17 µm	17 µm
Detector Time Constant	12 ms (typical)	
Measurement		
Object Temperature Range	-25°C to 100°C (-13°F to 212°F) -40°C to 550°C (-40°F to 1022°F)	
Accuracy	±5°C (±9°F) or 5% of reading	
Ethernet		
Ethernet Type	Gigabit Ethernet, control and image	
Ethernet Standard, Connector	IEEE 802.3, RJ-45	
Ethernet Communication	GigE Vision ver. 1.2, Client API GenICam compliant	
Ethernet Image Streaming	8-bit monochrome @ 60 Hz	8-bit monochrome @ 30 Hz
	Signal linear/DDE; Automatic/Manual; Flip H&V	
Bit Rate	14-bit 320 x 256 @ 60 Hz	14-bit 640 × 512 pixels @ 30 Hz
	Signal linear/DDE; Temperature linear GigE Vision & GeniCam compatible	
Ethernet Power	Power over Ethernet, PoE IEEE 802.3af class 0 power	
Ethernet Protocols	TCP, UDP, ICMP, IGMP, DHCP, GigEVision	
Digital Input/Output		
Digital Input	1× opto-isolated,"0" <1.2 VDC,"1" = 2–25 VDC	
Digital Output	1× opto-isolated, 2–40 VDC, max. 185 mA	
Digital I/O, Isolation Voltage	500 VRMS	
Digital I/O, Supply Voltage	2 – 40 VDC, max 200 mA	
Digital I/O, Connector Type	12-pole M12 connector (shared with digital synchronization and external power)	
Synchronization In	Frame Synch In to control camera 1x, non-isolated	
Synchronization In Type	LVC Buffer @ 3.3 V,"0" <0.8 V,"1" >2.0 V	
Synchronization Out	Frame Synch Out to control another FLIR Ax5 unit 1x, non-isolated	
Synchronization Out Type	LVC Buffer @ 3.3 V,"0" = 24 MA max,"1" = –24 mA max	
Digital Synchronization Connector Type	2-pole M12 connector (shared with Digital I/O and External power)	
Power System	**A35**	**A65**
External Power Operation	12/24 VDC, < 3.5 W nominal < 6.0 W absolute max	
External Power Connector Type	12-pole M12 connector (shared with Digital I/O and Digital Synchronization)	
Voltage	Allowed range 10 – 30 VDC	

Environmental Data		
Operating Temperature Range	–15°C to 60°C (5°F to 140°F)	
Storage Temperature Range	–40°C to 70°C (–40°F to 158°F)	
Humidity (Operating and Storage)	IEC 60068-2-30/24 h 95% relative humidity 25°C to 40°C (77°F to 104°F)	
EMC	EN 61000-6-2 (Immunity), EN 61000-6-3 (Emission), FCC 47 CFR Part 15 Class B (Emission)	
Encapsulation/Bump/Vibration	IP 40 (IEC 60529), 25 g (IEC 60068-2-27), 2 g (IEC60068-2-6), MIL-STD810G	
Physical Data		
Camera Size (L x W x H)	7.5, 9, and 13 mm lenses: 104.1 × 49.6 × 46.6 mm (4.1 × 1.9 × 1.8 in) 25 mm lens: 107.8 × 49.6 × 46.6 mm (4.2 × 1.9 × 1.8 in)	
	A35 w/ 50 mm lens: 141.1 × 58.4 × 58.4 mm (5.7 × 2.3 × 2.3 in)	A65 w/ 50 mm lens: 144.1 × 58.4 × 58.4 mm (5.7 × 2.3 × 2.3 in) A65 w/ 100 mm lens: 196.4 × 82.0 × 82.0 mm (7.7 × 3.2 × 3.2 in)
Tripod Mounting	UNC ¼"-20 (three sides)	
Base Mounting	4 × M3 thread mounting holes (bottom)	
Housing Material	Magnesium and aluminum	
Packaging		
Contents	Thermal imaging camera with lens, base support, printed documentation (some models include focus adjustment tool)	

Part Number	Camera
73309-0102	FLIR A35 f=9 mm with SC kit
83225-0101	FLIR A35 FOV 13 (60 Hz)
83213-0102	FLIR A35 FOV 25 (60 Hz)
83207-0102	FLIR A35 FOV 45 (60 Hz)
83250-0101	FLIR A35 FOV 6.5 (60 Hz)
83209-0102	FLIR A35 FOV 69 (30 Hz)
73413-0102	FLIR A65 f=13 mm with SC kit (30 Hz)
73513-0102	FLIR A65 f=13 mm with SC kit (7.5 Hz)
75050-0101	FLIR A65 FOV 12.4 (30 Hz)
75025-0101	FLIR A65 FOV 25 (30 Hz)
75013-0101	FLIR A65 FOV 45 (30 Hz)
75010-0101	FLIR A65 FOV 6.2 (30 Hz)
75007-0101	FLIR A65 FOV 90 (30 Hz)

Specifications are subject to change without notice. For the most up-to-date specs, go to www.flir.com

CORPORATE HEADQUARTERS
FLIR Systems, Inc.
27700 SW Parkway Ave.
Wilsonville, OR 97070
USA
PH: +1 866.477.3687

NASHUA
FLIR Systems, Inc.
9 Townsend West
Nashua, NH 03063
USA
PH: +1 866.477.3687

LATIN AMERICA
FLIR Systems Brasil
Av. Antonio Bardella, 320
Sorocaba, SP 18085-852
Brasil
PH: +55 15 3238 8070

CANADA
FLIR Systems, Ltd.
3430 South Service Road, Suite 103
Burlington, ON L7N 3J5
Canada
PH: +1 800.613.0507

www.flir.com
NASDAQ: FLIR

17-1683-INS-AUT

FLIR® The World's Sixth Sense®

Appendix D

Technical Drawings of the Camera Support

D.1 Definition Drawing of the Rectangular Connection Part

D.2 Definition Drawing of the Camera Connector

D.3 Exploded view of the Camera Support

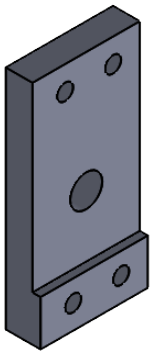

UNLESS OTHERWISE SPECIFIED: DIMENSIONS ARE IN MILLIMETERS SURFACE FINISH: TOLERANCES: LINEAR: ANGULAR:	FINISH:	DEBURR AND BREAK SHARP EDGES	DO NOT SCALE DRAWING / REVISION

	NAME	SIGNATURE	DATE
DRAWN		Diana Martins	
CHK'D			
APPV'D			
MFG			
Q.A			

TITLE:

Retangular connecting part

MATERIAL:	DWG NO.	A4
WEIGHT:	Scale 1:1	SHEET 1 OF 1

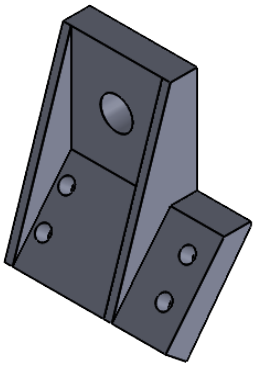

VIEW A
SCALE 1 : 1

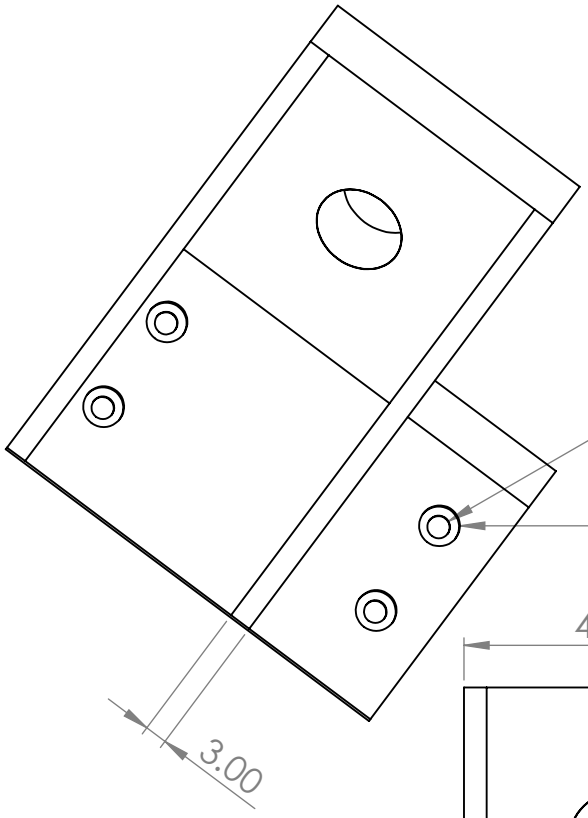

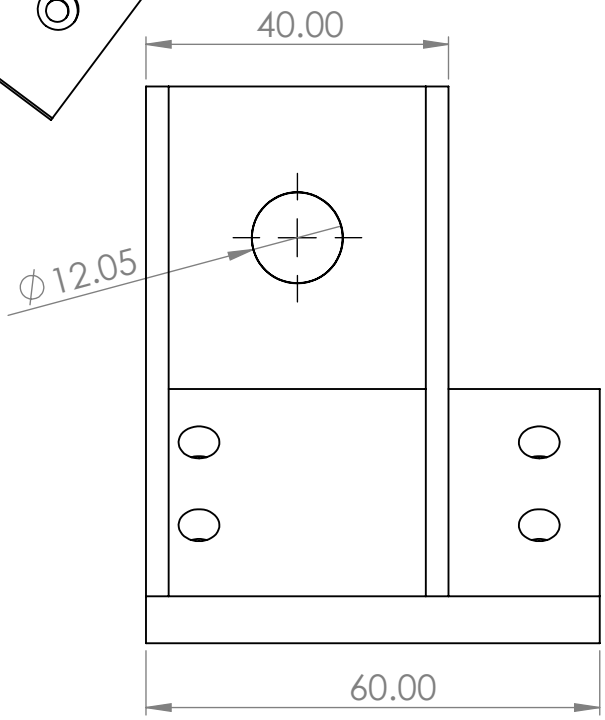

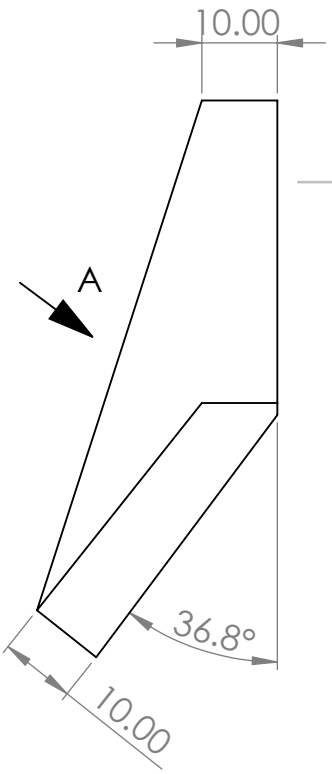

UNLESS OTHERWISE SPECIFIED: DIMENSIONS ARE IN MILLIMETERS SURFACE FINISH: TOLERANCES: LINEAR: ANGULAR:		FINISH:		DEBURR AND BREAK SHARP EDGES		DO NOT SCALE DRAWING	REVISION
	NAME	SIGNATURE	DATE			TITLE:	
DRAWN		Diana Martins				Camera Connector	
CHK'D							
APPV'D							
MFG							
Q.A				MATERIAL:		DWG NO.	A4
				WEIGHT:		Scale 1:1	SHEET 1 OF 1

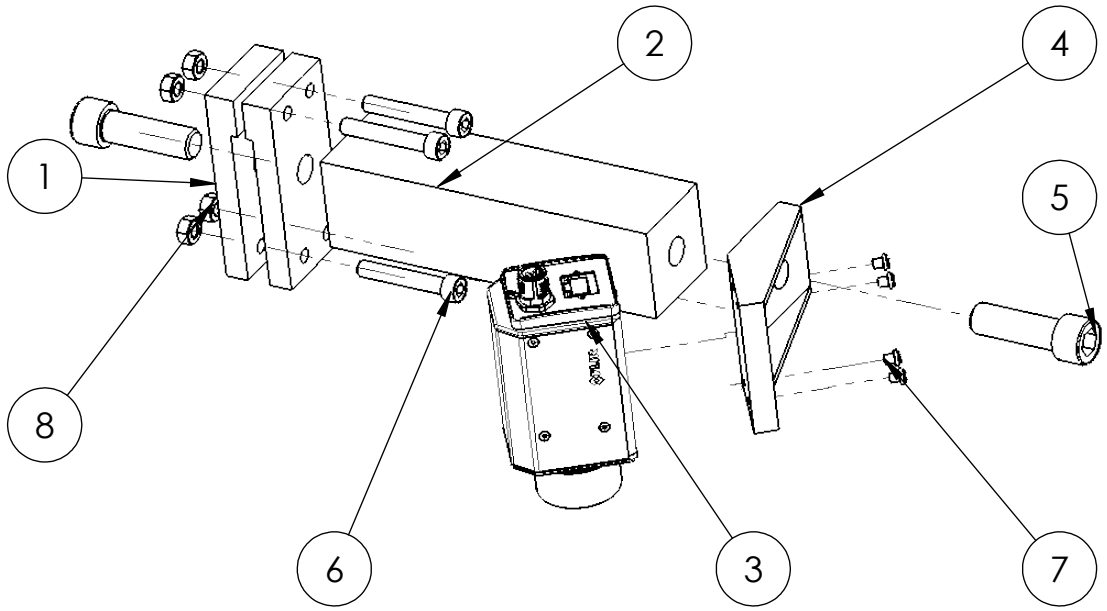

ITEM NO.	PART DESIGNATION	MATERIAL	DESCRIPTION	QTY.
1	Rectangular connecting piece	ABS Plastic		2
2	Profile 45x45 - 150 mm	Aluminium		1
3	Thermal camera FLIR A35			1
4	Camera connector	ABS Plastic		1
5	Socket head screw		ISO 4762 M12 x 40	2
6	Socket head screw		ISO 4762 M6 x 40	4
7	Pan head screw		ISO 7045 - M3 x 4	4
8	Hex nut		ISO 4032 - M6	4

Scale 1:3

UNLESS OTHERWISE SPECIFIED:
DIMENSIONS ARE IN MILLIMETERS
SURFACE FINISH:
TOLERANCES:
LINEAR:
ANGULAR:

FINISH:

DEBURR AND BREAK SHARP EDGES

REVISION

Scale 1:3

	NAME	SIGNATURE	DATE
DRAWN		Diana Martins	
CHK'D			
APPV'D			
MFG			
Q.A			

TITLE:

Exploded view of the camera support

MATERIAL:

DWG NO.

A4

WEIGHT:

SHEET 1 OF 1

Appendix E

Technical Drawing of the Printed Object

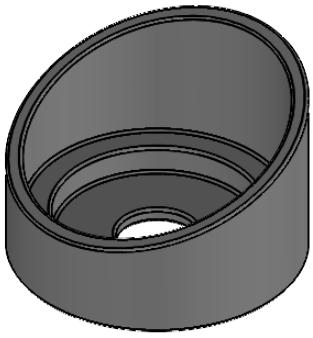

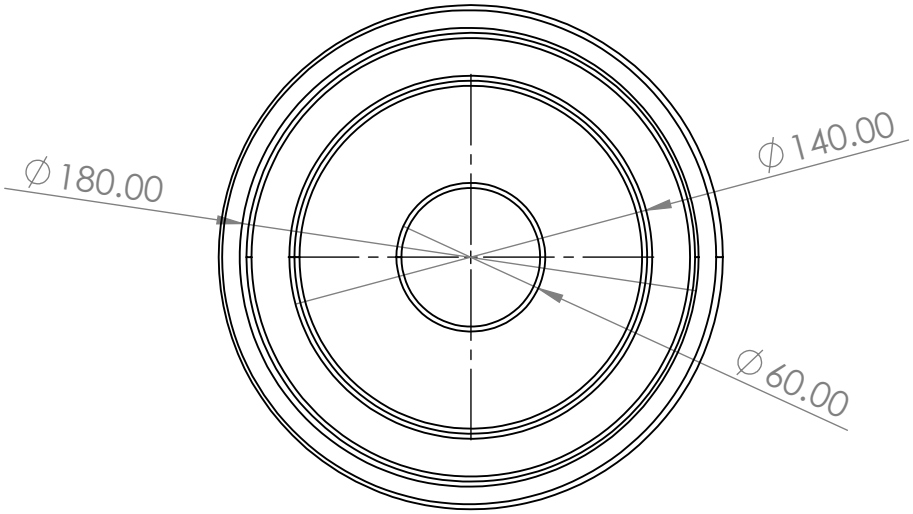

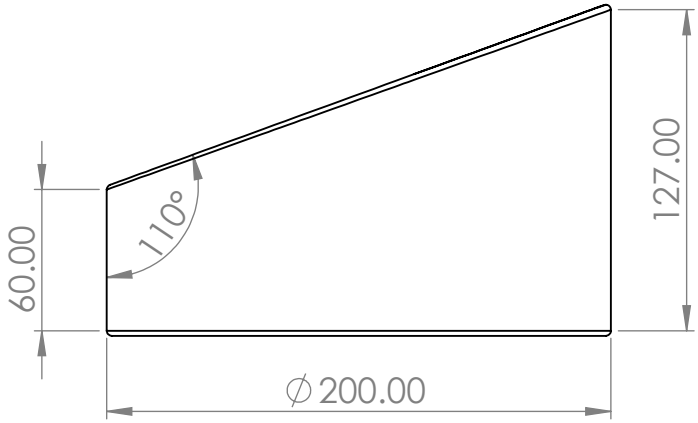

UNLESS OTHERWISE SPECIFIED: DIMENSIONS ARE IN MILLIMETERS SURFACE FINISH: TOLERANCES: LINEAR: ANGULAR:		FINISH:		DEBURR AND BREAK SHARP EDGES		DO NOT SCALE DRAWING	REVISION
	NAME	SIGNATURE	DATE			TITLE:	
DRAWN		Diana Martins				Printing Object	
CHK'D							
APPV'D							
MFG							
Q.A				MATERIAL:		DWG NO.	A4
				WEIGHT:		Scale 1:3	SHEET 1 OF 1

Appendix F

Average Temperature Evolution during the process

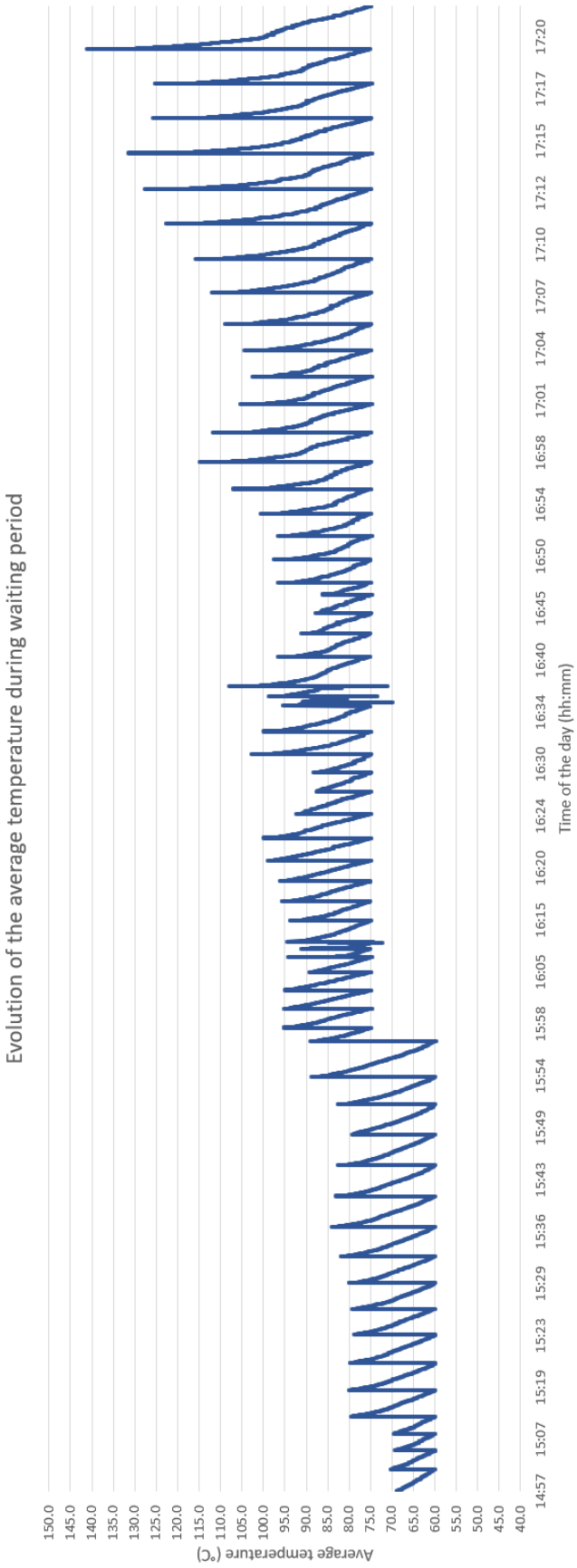

Figure F.1: Evolution of the average temperature during the printing